5-2018

A Study about the Effect of Addition of Carbon Nanofibers on the Strain-Rate Sensitivity of Thermoplastic Polymer Matrix Nanocomposites Manufactured by Ultrasonication Process

Rohit Tandon
Clemson University, rohittandon93@gmail.com

A STUDY ABOUT THE EFFECT OF ADDITION OF CARBON NANOFIBERS ON THE STRAIN-RATE SENSITIVITY OF THERMOPLASTIC POLYMER MATRIX NANOCOMPOSITES MANUFACTURED BY ULTRASONICATION PROCESS

A Thesis
Presented to
the Graduate School of
Clemson University

In Partial Fulfillment
of the Requirements for the Degree
Master of Science
Mechanical Engineering

---

by
Rohit Tandon
May 2018

Accepted by:
Dr. Hongseok Choi, Committee Chair
Dr. Georges Fadel
Dr. Oliver J. Myers

ABSTRACT

Thermoplastic polymers have been widely used in the industry due to their high toughness and impact resistance along with their remolding capabilities as compared to thermoset polymers, which also makes them an attractive choice for polymer composites. Many desirable features of thermoplastic polymers like ease of processing, low weight and cost, and corrosion resistance make thermoplastics a viable option for applications in the automotive, aerospace, sporting goods and many other industries. To further increase the mechanical, thermal and electrical properties of thermoplastic polymers, nanomaterials are added to the polymer matrix that can improve these properties at very low loading levels as compared to conventional fillers.

In this work, Polypropylene (PP), a semi-crystalline thermoplastic known for its balance of strength, modulus and chemical resistance has been used as the polymer matrix. It is one of the most widely used thermoplastic polymers in several industries as it shows a good combination of stiffness, toughness and creep resistance along with being light-weight and cost effective. Carbon Nanofibers have been used as the nanomaterial in this work for understanding the effect of nanomaterials to mechanical properties of the polymer matrix.

Thermoplastics, including Polypropylene, exhibit varying mechanical properties based on the different loading rates that they are subjected to. Polymers experience stress relaxation at constant strains and creep under constant load due to their viscoelastic nature, i.e. they exhibit properties both of an elastic solid and a viscous liquid. The stress relaxations are distinct for different polymers and are divided into unique processes that

lead to a strain-rate dependency of the semi-crystalline polymer which has been studied in this work.

To fabricate these nanocomposites, ultrasound-assisted mixing has been used to reduce the processing time, utilizing the well-known dispersive qualities of ultrasound in solutions. Ultrasound-assisted mixing, as a processing technique for directly manufacturing polymer matrix nanocomposites has not been studied much in the literature. Ultrasonication in polymer solutions can also be responsible for polymer degradation due to its cavitation effects. To understand the effects of dispersion and polymer degradation caused by ultrasonication, mechanical mixing of polymer solutions has also been used as a counterpart to the ultrasonication process.

For studying the effects of processing and nanomaterial addition on the strain-rate dependency of the polymer matrix, tensile tests were conducted using injection molded dog-bone samples made as per the ASTM D638 V standards. For manufacturing these dog-bone samples, an injection mold was designed and manufactured based on the statistical analysis of simulations conducted using Moldex 3D, a polymer melt-flow simulating software. Tensile strength, elongation at break and the tensile modulus values have been used as the basis for comparison. To understand the strain rate dependency of the polymer and its nanocomposite, quasi-static strain rates varying from 10^{-4} to 10^{-1} s^{-1} have been utilized. Thermal Gravimetric Analysis (TGA) has also been conducted for studying the effects on the thermal properties of the polymer.

Polypropylene has shown a visible response to varying strain rates as expected, as the strength and modulus of the polymer increases with increasing strain rate, while the

elongation decreases. Ultrasonically processed polymer and its nanocomposites also show a similar linearity in the strain-rate dependency as the pure polymer. The effects of ultrasonication on the polymer degradation have been presented along with the effects of addition of nanomaterials. Mechanical and thermal properties have been discussed based on the tensile tests and TGA. Conclusions and future recommendations are presented based on the observations done.

ACKNOWLEDGMENTS

Firstly, I owe my deepest gratitude to my advisor, Dr. Hongseok Choi, for motivating me towards this thesis and for his patience and invaluable support for my work. His guidance and immense knowledge has helped me get through my thesis and I could not have imagined a better mentor for my graduate studies.

Besides my advisor, I would like to thank my committee members; Dr. Georges Fadel and Dr. Oliver J. Myers for their insightful comments and encouragement for the completion of my work.

I would also like to acknowledge Dr. Srikanth Pilla who provided me the access to his lab and research facilities. I owe a sincere thanks to my fellow labmates at Clemson Advanced Manufacturing and Materials Processing (CAMMP) lab for their support and assistance.

Finally, this thesis would not have been possible without the love and support of my family, especially my parents Saroj Tandon and Chander Pal Tandon, who have kept me strong and motivated me throughout my graduate degree.

TABLE OF CONTENTS

Page

Table of Contents (Continued)

Page

LIST OF TABLES

LIST OF FIGURES

List of Figures (Continued)

Figure Page

CHAPTER I

INTRODUCTION

1.1. Background

Thermoplastic polymers have been widely used in the industry due to their advantages, as compared to thermoset polymers. Thermoset polymers can only be shaped once after heating, and any further heat applied to them leads to degradation. Whereas, thermoplastic polymers can be easily reformed into different shapes with the application of heat. Thermoplastics also have increased toughness with high ductility and their impact resistance can be 10 times as high as that of thermoset polymers. For such reasons, thermoplastic materials are an attractive matrix choice for making polymer composites.

Characteristic features of the polymer composites such as low weight, ease of processing, low cost, and corrosion resistance make them desirable for a variety of applications such as automobile components, aerospace components, sporting goods, and so on. Organic or inorganic fillers are commonly added to polymeric systems. Fillers are generally added to enhance the physical and/or chemical properties of the polymers. In the past three decades, polymeric nanocomposites have seen great development. Nanocomposites are materials in which the fillers have at least one dimension in the nanoscale. The final product does not need to be in the nanoscale. It can also be a macro or micro scale composite.

Nanomaterials can be classified into three main categories: layered materials which include layered silicate, graphite, and other layered materials; particles which

include metals, silica, and other inorganic and organic particles; and fibrous materials which include nanotubes and nanofibers. In this study, we will mainly focus on fibrous materials, specifically Carbon Nanofibers(CNF). Nanomaterials have a much larger surface area as compared to their volume [1]. A change in fibrous material diameter from micrometer to nanometer changes the surface area to volume ratio by three orders of magnitude [2]. As surface properties govern a lot of physical and chemical properties [3], a nanomaterial with a same composition as a micro or macro-dimensional material will have very different properties. Thus, nanomaterials can improve the properties of polymers with very low filler loading levels as compared to conventional micro-scale fillers. Nanomaterials can affect the tensile strength, toughness, heat deflection temperature, stiffness, barrier properties, and fire retardancy of polymers. For these reasons nanomaterials are a desirable addition to polymers for light-weight polymer composite industry.

The thermoplastic polymer being used in this study is Polypropylene (PP). It is a semi-crystalline polymer that is well known for its balance of strength, modulus and chemical resistance. Polypropylene is widely used in the automobile industry, as well as many potential applications in appliances and other commercial products where stiffness, creep resistance, and toughness are needed along with light-weighting and cost savings. Polypropylene is a desirable material for automotive components as it is capable of withstanding large strain levels prior to failure.

Polymers, especially thermoplastics, have a tendency of exhibiting different mechanical properties based on the different loading rates that are applied to them. For

this reason, there has been increasing interest in understanding the mechanical properties of polymers and polymeric systems at high loading rates [4–8]. This interest has been spiked for providing the essential data required by designers for practical applications of these materials, keeping into consideration the rate dependence of the deformation mechanisms and their mechanical properties. Polymers are being increasingly used in the aerospace and automotive engineering industry, where strain rates as high as 300 s^{-1} can be experienced [9]. Polymers have a viscoelastic nature, i.e. they exhibit some properties similar to both elastic solids and viscous liquids due to some relaxation processes that will be explained in Chapter 2. This viscoelastic nature, and its effects thereof, have an influence on the polymer properties when they are characterized at different strain rates during tensile loading. These intrinsic properties make the polymers' properties strain-rate dependent, and this dependency will be studied in this work.

Plastic components, specifically PP manufactured products, are usually made by injection molding process. It is a versatile operation for the mass production of complex plastic parts which is used to process 32% of all plastics. It is a cyclic process that utilizes plastic pellets or powder and forms it into the desired shape by driving the material under pressure into a cavity. There are two types of injection molding machines, Horizontal and vertical injection molding machines, as shown in Fig 1. Horizontal machines, shown in Fig 1(b), are the most commonly used machines in the industry, whereas vertical injection molding machines, as shown in Fig 1(c), are the ones that are used for special operations like manufacturing fragile parts that cannot be subjected to freefall after

ejection from the mold. In this study, a desktop vertical injection molding machine, shown in Fig 1.2 has been used.

In a typical injection molding process, the plastic is melted inside the barrel of the machine using heaters that surround the barrel for uniform heating. This molten plastic is then pushed out of the barrel, via a nozzle into the mold cavity with the help of a rotating and reciprocating screw. In the machine used for this study, the screw is replaced by a ram. The only difference a ram creates is causing less shear on the plastic because of no rotating actions of the screw geometry. Although a desktop version has been used in this study, the design and guidelines for injection molding have still been followed.

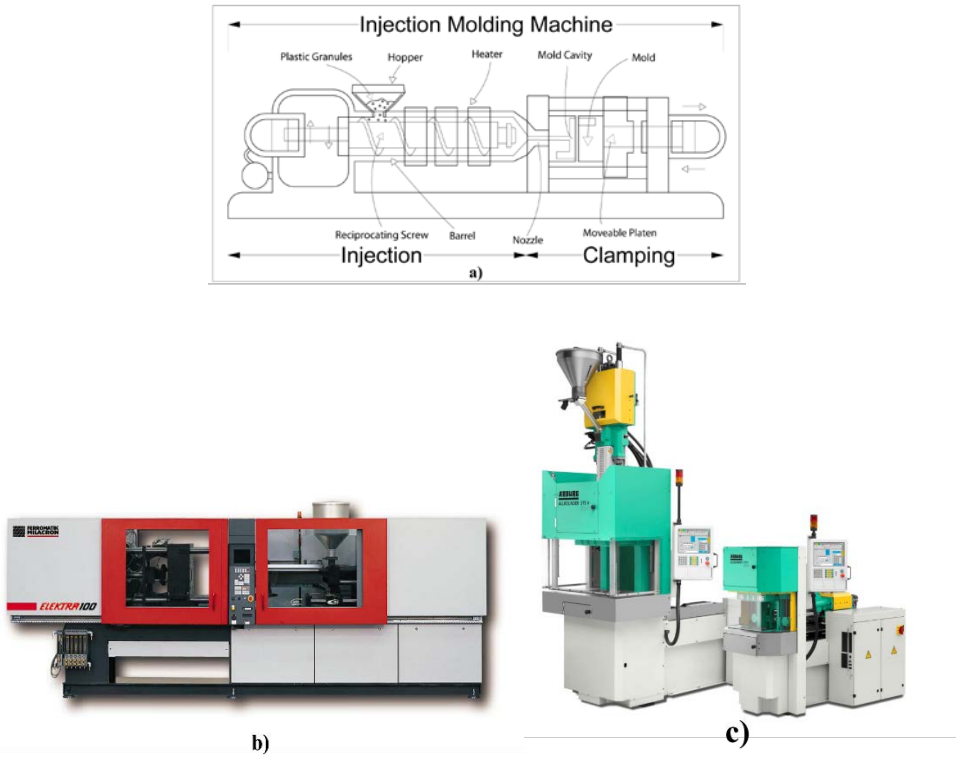

Fig 1.1: a) Schematic of an Injection molding machine, b) Horizontal Injection molding machine, c) Vertical injection molding machine.

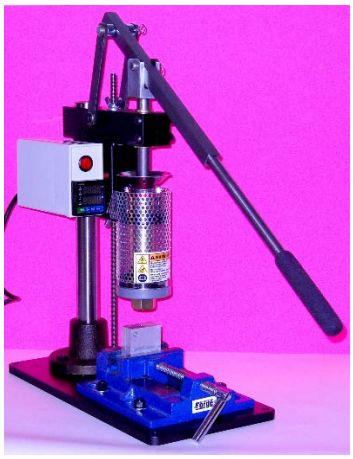

Fig 1.2: Vertical desktop injection molding machine used in the study

For the preparation of nanocomposites in this study, ultrasonication has been used for dispersion of nanofibers in the polymer. Ultrasound are sound waves above the frequency of 20kHz. Humans can hear sound waves with a frequency range from 20 Hz to 20kHz. Based on the application, ultrasound can be classified into two broad categories: power ultrasound and diagnostic ultrasound [10]. Frequencies in the range of 20 kHz to 2 MHz fall into power ultrasound which is used in applications such as ultrasonic cleaning, ultrasonic machining, ultrasonic material processing, and sonochemistry. Frequencies in the range of 2 MHz to 100 MHz fall into diagnostic ultrasound which is used mainly in non-destructive testing, SONAR or sonography.

For processing liquids, the ultrasound used is power ultrasound. Acoustic cavitation and acoustic streaming are generated by the interaction of the ultrasonic waves with liquids. Acoustic streaming is the generation of flow in the liquid during ultrasonic processing. This is caused by the attenuation of the ultrasonic wave, which can cause a loss of acoustic momentum that can lead to a jet-like flow in the liquid.

Acoustic cavitation is the generation of new surfaces in a liquid when ultrasonic waves are introduced in it [11]. In this definition, surfaces are the walls of the cavitation bubbles in the liquid, which require the acoustic pressure to be greater than the tensile strength of the liquid, that is the strength required for cavitating a liquid. But, the acoustic cavitation can be observed well below such acoustic pressures [12]. This is caused by the existence of seed nuclei, which are micro sized bubbles in liquids. By the process of rectified mass diffusion, dissolved gas from the surrounding liquid is transferred across the wall of cavitation bubble. This gas pressure inside the bubble is greater than the surrounding liquid pressure during the compression cycle and vice versa during the rarefaction cycle. The net flow of gas across the cavitation bubble is not zero during one complete acoustic cycle, as the surface area of the cavitation bubble changes between compression and rarefaction cycles. The cavitation bubble is smaller than the equilibrium size during the compression cycle and vice versa for the rarefaction cycle. The cavitation bubble is of equilibrium size when the gas pressure inside and outside the wall of the bubble are equal. As the net gas transfer is not zero, the bubble keeps on increasing in size until it finally implodes. This can cause conditions of high temperature and pressure [13] in the localized hotspot zones, but these conditions are short lived because of the rapid cooling rates.

1.2. Motivation and Objectives

Polymers are viscoelastic materials as explained above. For these materials, the relation between stress and strain is time dependent. Due to the viscoelastic nature of the polymers, a strain rate dependency is observed in them. This means that the mechanical

properties of the polymers depend upon the rate at which the load is applied to them. This strain rate dependent behavior is essential to study for a polymer as they are used in applications where there can be varying intensities of load which are applied for varying periods of time. To understand the behavior of the material under different strain conditions it is essential to test it under various strain rates for the mechanical property characterizations. For this reason, the pure PP and the PP/CNF nanocomposites have been tested at various strain rates. These results can help generate a model for the material behavior prediction at different strain loadings under quasi-static conditions. Thus, one of the objectives of this research is to study the strain rate dependency of PP and its nanocomposites so that their mechanical behavior can be characterized.

It is a well-known fact that exposure to ultrasound can cause polymer degradation. There is experimental evidence showing the cavitation effects of ultrasonication in polymer solutions on macromolecules. The hydrodynamic forces related with cavitation are responsible for the degradation, rather than the thermal and chemical effects associated with cavitation. During cavitation, the macromolecules get suspended in a field of eddies. Eddies are formed by the disintegration of elastic waves, generated by cavitation, due to their interaction within themselves and the medium. Due to eddy motion in this field, the molecule will experience motions of varying intensities and amplitudes. These motions can cause a dynamic force across the length of the molecule, which will degrade the molecule once it exceeds the bond strength [14].

One of the effects of polymer degradation is that it causes the molecular distribution to become much narrow [15,16] as the polydispersity is changed. It has also

been experimentally seen that molecular chain degradation only works with a limiting chain length. Studies have shown that polymers degrade rapidly at higher molecular weights and as the molecular weight decreases, it reaches a limiting value after which ultrasonication has no effect on the polymer in terms of degradation. This effect has been seen in polymers in general and has no variation due to the polymer type or chemistry. Studies have been done with macromolecules in solutions in both organic and inorganic polymers in organic and aqueous media [17–21].

Considering the above-mentioned effects of ultrasonication on polymers, the second objective of this work is to examine the response of the polymers after they have been processed ultrasonically, to study the effect of the process on the mechanical and thermal properties of the materials. On the other hand, ultrasound as a processing tool is considered to have good dispersion capabilities. Due to the cavitation bubble collapse and the acoustic streaming, ultrasonication can cause the de-agglomeration of CNFs and help with dispersing them across the polymer matrix. The nanofibers added to the polymer through the help of ultrasonication will have an effect on the mechanical properties of the pure polymer. Thus, the effect of addition of nanomaterials on the strain rate sensitivity will also be studied.

The research objectives of this work are hence explained as follows:

- To study the strain-rate sensitivity of PP and understand the effects of processing and nanomaterial addition to the matrix on the strain-rate dependency of the polymer.

- To study the effects of ultrasound-assisted processing on PP by analyzing the effect on the mechanical properties and thermal behavior of the polymer.

1.3. Outline of the thesis

The thesis has been divided into five chapter. Chapter 2 discusses an intensive literature review of the several topics covered in this thesis. The strain-rate dependency of polymers and the various mechanisms involved within this study have been discussed comprehensively. Ultrasound-assisted mixing and its effect on the polymer degradation have been studied in detail. The fabrication of several nanomaterials and their uses in polymeric systems have been discussed along with their applications in the industry. A brief introduction to Thermal Gravimetric Analysis and its applications in characterization of polymers has also been provided.

Chapter 3 talks about the experimental procedures for the fabrication and testing of the polymer and its nanocomposites. It also discusses extensively about the design and manufacture of an injection mold for creating the tensile dog-bone samples, needed for studying the mechanical properties of the polymer and its nanocomposites. The various material and equipment utilized in this thesis have also been mentioned in Chapter 3.

Chapter 4 talks about the results of the mechanical and thermal properties testing of the polymer and its nanocomposites. The results have been discussed based on the trends in the data obtained and also the intensive literature review conducted on these topics. The conclusions from these results have been presented in Chapter 5. Chapter 6 contains the potential future works related to this study.

CHAPTER II

LITERATURE REVIEW AND BACKGROUND

2.1. Strain Rate Effect in Thermoplastic Polymers

Polymers have a viscoelastic nature, i.e. they exhibit some properties similar to both elastic solids and viscous liquids due to various relaxation processes occurring through the polymer. Viscoelastic properties lie somewhere in between the properties of a perfectly elastic solid and a viscous liquid. A perfectly elastic solid, when under the application of stress, stores the work done on it in the form of energy of deformation and then releases it when the stress is removed, thereby returning to its original shape. Whereas, the work done by shearing stresses on a viscous liquid flow is dissipated as heat and the removal of the stress, although ceases the flow, but the liquid has no tendency to return to its original state.

Due to these viscoelastic properties, polymers usually experience stress-relaxation at constant strains and creep under constant load [22]. Stress relaxation occurs unnoticed during constant strains and is an intrinsic property of polymers, which has visible effects only after the stress has been removed. Creep on the other hand, is the response of the viscoelastic flow of the polymer under a constant load that causes a visible deformation even during the application of load. Both the properties are temperature and time dependent.

Mechanical models that use Hooke's law obeying elastic springs and dashpots that contain Newton's law obeying viscous liquids are used to represent the viscoelastic

behavior of polymers. Two of the simplest models that use these concepts have been explained below:

- **Maxwell Model**:

This model uses the spring and the dashpot connected in series as shown in Fig 2.1 (a), to explain viscoelasticity. In this case, when a fixed strain is applied instantaneously, the spring extends immediately and a stress is produced in it. This stress is also applied to the dashpot, but there is no instantaneous response from the dashpot, as is the case with the spring. It starts displacing at a decreasing rate proportional to the stress, until the stress in the spring is decayed to zero and the dashpot's displacement is the same as the original spring displacement. This model, therefore is majorly concerned with only stress relaxation and not the creep mechanism as the spring remains at constant length under constant stress, and the dashpot displaces at a constant rate. Also, the decay of the stress to zero in the spring is not usually seen in real polymers, they only drop to a certain value, which will be explained later.

- **Kelvin or Voigt Model:**

This model explains viscoelasticity by the help of a spring and a dashpot connected in parallel as shown in Fig 2.1 (b). Under the application of a sudden fixed stress, the dashpot cannot be displaced instantaneously and therefore there is no change in the length of the spring and it carries no stress. As the dashpot starts displacing at a decreasing rate, the spring starts to take up some of the stress and this goes on until the spring and the dashpot reach their maximum displacement and the spring can take up the whole load. This model is thus majorly concerned with creep and not stress-relaxation.

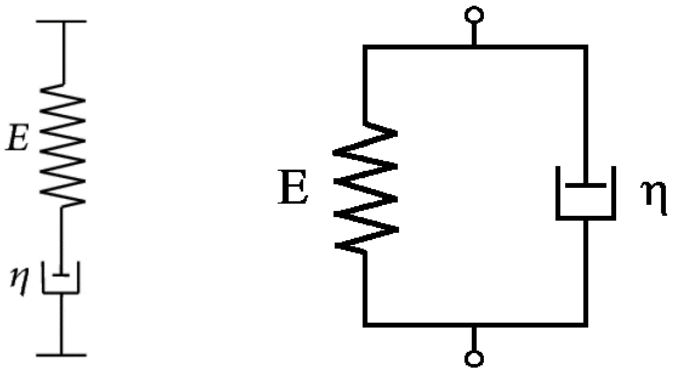

Fig 2.1: Spring and dashpot arrangement a) in series: Maxwell model, b) in parallel: Voigt model.

To explain both stress relaxation and creep in a single model, the standard linear solid model can be used. It combines a spring in parallel with a Maxwell element as shown in Fig 2.2. During stress relaxation, spring 1 maintains original strain, whereas E_2 and η are responsible for stress relaxation. Also, as can be proven here, the stress relaxes to eE_1 and not zero, where 'e' is the strain. During creep, there is an instantaneous response from the two springs as they are in parallel and can extend immediately. Thus, this model explains a polymer in a much better sense but still none of these models are capable of explaining the complete behavior of real polymers. Real polymers have various different stress relaxation mechanisms which require a lot of different elements for effective explanation of the behavior. One of the examples of models to explain the complicated behavior can be using a number of Maxwell elements in parallel, each of which have their own relaxation times, and the stress is equivalent to the sum of stresses in individual element [22].

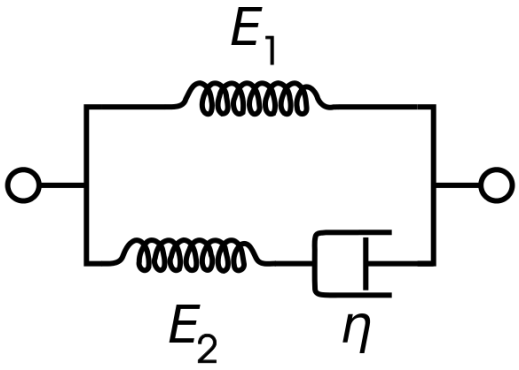

Fig 2.2: Standard Linear Solid Model.

When stress is applied to a polymer, the internal structure relaxes to achieve a state of equilibrium under the applied stress. This relaxation can be achieved by a change in the proportions of various orientational and conformational states of the molecules. The rates of transitions between these certain groups of conformations are equal to the relaxation rates that are observed during certain mechanical measurements. The transition rates of chain conformations are widespread over a range. They can be as rapid as local rearrangements in few adjacent molecules, or they can be time-consuming if widespread over extended sequences. The relaxatory modes that are related to the whole chain can be molar mass dependent as the relaxation needs to travel large distances [23]. These relaxatory modes are segregated into several accumulated reaction rate zones. These zones are denoted by α, β and γ, where α has the lowest transitions rates and γ has the highest.

The α-process in a semi-crystalline polymer is of composite nature. It combines two relaxation processes, one in the crystallites and one in the amorphous zones which are coupled together [23]. Mechanical relaxation occurs due to an additional shearing of the

amorphous zones which has a prerequisite of a chain movement through the crystallites. The elastic modulus for the polymer is thus dependent on the nature and extent of these changes.

The Ree-Eyring theory [24] is one of the most important analytical models that explains the polymer plasticity and captures the yield behavior across this transition. When applied to polymer plasticity, the Ree-Eyring theory assumes that some specific degrees of freedom of the polymer chains can be responsible for the multiple rate-activated processes in a polymer. Thus, the molecular level motions can be used to explain the yield behavior transition. At high strain rates, a specific degree of freedom of the polymer chains can be suddenly restricted which can cause the resulting processes to contribute to the resistance to deformation in the overall material. The Ree-Eyring theory mostly only considers the α-process and the most important β-process in thermoplastic polymers [25].

Mulliken et al. [25] talk about the strain-rate dependency of polycarbonate (PC) and poly(methyl methacrylate) (PMMA) based on experimental work at several high strain-rates utilized by different testing techniques. The results have been discussed based on a physical model based on the model introduced first by Boyce et al. [26] that includes a linear elastic spring and a viscoelastic dashpot in series with a nonlinear Langevian spring in parallel.

There are several phenomenological models that are used to describe the strain-rate dependency of polymers. Several groups have worked on understanding the behavior of polymers at high strain rates to understand the material behavior in various applications

across the industry. Pouriayevali et al. [27] talk about the strain rate effects seen in Nylon 6 based on a constitutive model describing the elastic-viscoelastic-viscoplastic framework that illustrates the rate and temperature dependent response of Nylon 6 at quasi-static as well as high rate large deformations. The Hyperelasto-Visco-Hysteresis (HVH) [28,29] model is a different model that utilizes the viscous properties of the material to explain the strain rate dependency. Zrida et al. [4] use the HVH model to explain the strain rate dependency based on the linear evolution of characteristic recorded times in Maxwell branches. They also conclude that the strain rate dependency can be attributed to only the viscous part in the HVH model. The strain rate dependency of isotactic PP (iPP) and modified iPP containing ethylene-propylene rubber have been discussed by Gensler et al. [30] using the different fracture behavior of the polymer. A ductile-brittle transition has been seen with an increase in the test speed, due to the differences in the type of the fracture. The loss in ductility with increase in strain rates has been attributed to a change in the deformation mechanisms.

In case of semi-crystalline polymers like PP, the G'Sell-Jonas model is frequently used [31–34] to describe the strain rate dependent behavior of the polymer. Schobig et al. [5] talk about the behavior of glass-fiber reinforced PP and polybutene-1 (PB-1) at high strain rates based in the G'Sell-Jonas model. The G'Sell-Jonas model is used to describe the dependence of flow curve on the strain, temperature and the strain-rate. It has been explained in the literature using the following equation:

$$\sigma\left(\dot{\varepsilon},\varepsilon,T\right)=K\left(\dot{\varepsilon}\right)^{m}e^{h\varepsilon^{2}}\left(1-e^{-W\varepsilon}\right)e^{\frac{a}{T}}$$

Here, K, m, a, W, h are material constants and T is the absolute temperature. $\left(1-e^{-W\varepsilon}\right)$ is the viscoelasticity, $\left(\dot{\varepsilon}\right)^{m}$ is the viscoplasticity, $e^{\frac{a}{T}}$ is the influence of temperature and $e^{h\varepsilon^2}$ is the strain hardening [5].

2.2. Ultrasound-assisted mixing

Just like thermochemistry and piezochemistry, sonochemistry can be considered a general activation technique. Sonochemistry is a field that uses ultrasound as a tool for general chemistry. Ultrasound that is broadly classified as a sound above 20 kHz to 100 MHz can be divided into three categories:

- Conventional power ultrasound which ranges from 20-100 kHz. This is generally used for industrial applications and sonochemistry.
- Extended sonochemistry applications that are performed within the range of 100 kHz to 2 MHz, and
- Diagnostic ultrasound which is low power and high frequency within the range of 5 to 10 MHz

In general, the frequencies between 20-40 kHz are too low to interact with the material at the molecular level and not even enough for the excitation of rotational motion. But, these frequencies can generate enough acoustic energy needed to induce cavitation in liquids. This phenomenon causes the production of microbubbles in the liquid when a large negative pressure is applied on the liquid. There are three distinct ways to achieve cavitation in a liquid namely, by fluid flow i.e. hydrodynamic cavitation; by ultrasound i.e. acoustic cavitation; or by depositing a large amount of energy into the

liquid by using lasers. In this study, we will be using the acoustic cavitation to achieve the dispersion and distribution of nanofibers into the polymer matrix.

Ultrasound alternately compress and stretch the liquid's molecular structure which causes a change in the average distance between the molecules as they tend to oscillate about their mean position. By the help of the acoustic pressure in the liquid, the distance between the molecules exceeds to a point where the molecules are unable to hold the liquid intact. This causes the creation of voids which are the cavitation bubbles, and this point is known as the cavitation threshold [35]. Sonochemistry can only occur above the cavitation threshold. Some advantages of using ultrasound for conventional solid/liquid reactions are:

- Ultrasonication breaks up the surface structure of the material to allow penetration of the reactants.
- Degradation of large molecules, as explained above, helps reduce the particle size and thus results in an increase of the surface area.
- An important advantage that is made use of in this study is the reduction in the induction time.

One of the mechanical effects of ultrasonication that needs to be studied is the degradation of the long polymer chains because of shock waves and microstreaming produced by cavitation bubble collapse. The collapse of the cavitation bubble causes the wall velocity to approach the speed of sound and the trapped gas inside the bubble causes sudden deceleration of the wall motion. Thus, shockwaves are generated due to the

release of an intense pressure wave. Eddies are formed by the disintegration of these elastic waves, generated by cavitation, due to their interaction within themselves and the medium. During cavitation, the macromolecules get suspended in a field of eddies. Due to eddy motion in this field, the molecule will experience motions of varying intensities and amplitudes. These motions can cause a dynamic force across the length of the molecule, which will degrade the molecule once it exceeds the bond strength [14]. The scission of macromolecules occurs if the energy imparted from the bubble implosion cannot be dissipated by the macromolecule [36]. Microstreaming is also caused due to the induced fluid flow and the promotion of radiation forces on the particles caused by the oscillation and collapse of the cavitation bubbles. These phenomena cause the degradation of the long polymer chains and thus their effect on the mechanical properties of the polymer will be studied here. There are two process that result from ultrasonication that can result in polymer degradation [35]:

- First one, independent of the polymer concentration, is radical generation which occurs along the complete polymer chain randomly.

- Second one, dependent on the polymer concentration, is mechanical breakdown because of the shear forces due to the cavitation collapse in the aqueous phase.

Ultrasound can enhance the rate of polymerization in polymers by acting as an initiator and breaking the chemical bonds of molecules due to the intense conditions generated by acoustic cavitation [37]. One of the effects of polymer degradation is that it causes the molecular distribution to become much narrow [15,16] as the polydispersity is changed. It has also been experimentally seen that molecular chain degradation only

works with a limiting chain length. Studies have shown that polymers degrade rapidly at higher molecular weights and as the molecular weight decreases, it reaches a limiting value after which ultrasonication has no effect on the polymer in terms of degradation. This effect has been seen in polymers in general and has no variation due to the polymer type or chemistry. Studies have been done with macromolecules in solutions in both organic and inorganic polymers in organic and aqueous media [17–21].

Sonochemical method of synthesizing nanocomposites is the by far the most superior over all existing techniques [38]. Ultrasound can cause intense shearing that can help in the dispersion of nanomaterials, such as graphene sheets, in the polymer matrix. This uniform dispersion due to ultrasonication can result in better mechanical and electrical properties of the nanocomposites, as compared to conventional methods [37]. Nanocomposites with expanded graphite in an anhydride cured epoxy resin matrix have been prepared by Yasmin et al [39]. The nanocomposites were prepared with a combination of sonication and shear mixing which helped in the formation of nano-size graphite sheets during polymerization from the expanded graphite sheets. They have also reported that sonication time effects the resultant nanocomposites' properties.

Multiwalled carbon nanotubes have been dispersed in polystyrene solution using ultrasonication by Safadi et al [40]. Although aggressive chemical modifications are needed for dispersing carbon nanotubes using conventional methods, they have reported that ultrasonic energy can disperse the MWCNTs in the composites without any chemical pretreatment. For making CNT nanocomposites, a metastable suspension of nanotubes dispersed in a suitable solvent is mixed with polymers using ultrasound [41]. This helps

in improving the load transfer capabilities of CNT/polymer nanocomposites by solvent blending method.

2.3. Thermoplastic Nanocomposites

Polymers have been widely used in the industry since a long time because of their intrinsic properties such as good insulation, light weight, ease of processing and good insulation. These properties have made polymers useful in the automobile, aerospace, packing and construction sectors. These polymer properties can be further enhanced and modified with the addition of Nano-fillers and fibers to the polymer matrix.

Nanoparticles, such as nanoclays have been in use since the 1950's. They were then used for controlling the flow of the polymer and for maintaining the constitution of gels. A nanomaterial is any material which has at least one dimension in the nanoscale. Nanoscale materials have a large surface area for a given volume [1]. Surfaces and surface properties govern a lot of physical and chemical properties, and thus nanomaterials have significantly different properties from a macro level material. Nanocomposites are solid multiphase materials where at least one of the phases has at least one dimension <100nm. Because of the nanomaterials, nanocomposites are very different from conventional composites because of the exceptionally high surface area-to-volume ratio, i.e. aspect ratio of the nanomaterials. In this new age, light-weighting along with strength and toughness is a highly-desired property. This calls for improvement in properties of the existing materials or use of new materials for achieving the goal. Nanomaterials offer an improvement in the properties of the existing polymers with very low filler loading levels as compared to conventional fillers.

Nanomaterials can increase the tensile strength, toughness, heat deflection temperature, and stiffness of a material. They can also increase the barrier properties of a material as the fillers cause the flow of gases and vapor to slow down by creating a tortuous path [42]. The increase in barrier properties can help use these nanocomposites in packaging and automotive industry. They are already used for food packaging, tire inner-liners and beer bottles and can be used in automotive fuel system components such as seals, gaskets, and hoses [43].

Nanocomposites also help in fire-retardant applications. Building Fire and Research Laboratory (BFRL) and National Institute of Standards and Technology (NIST) are working on protective fabrics for clothing since the thermal conductivity of CNTs are at least three orders of magnitude greater than other materials along the tube axis [44]. Nanocomposites, especially the ones using CNTs as nanofillers have also been known to enhance the conductivity of the composites.

Nanomaterials can be classified into three main categories: layered materials which include layered silicate, graphite and other layered materials; fibrous materials which include nanotubes and nanofibers; and other particles which include metals, silica, and other inorganic and organic particles. In this work, we will only be discussing fibrous materials because of their relevance to the study.

2.4. Nanomaterials and their Nanocomposites

2.4.1. Carbon Nanofibers

Carbon Nanofibers (CNFs) are one of the most important members of Carbon Fibers (CFs), and they have applications in various fields as promising materials for

reinforcement, energy conversion and storage, and self-sensing devices [45–47]. CNFs are different from CFs in some ways. The major difference is the size of the fibers. CFs have diameters of several micrometers whereas CNFs have diameters in the range of 50-200 nm. The lengths of the fibers are in the range of 50-100 μm resulting in aspect ratios of around 250-2000 [48]. The two types of fibers also have different structures mainly because of the different methods of preparation. CFs are mostly PAN or pitch based fibers that are made under a variety of conditions including variations in heat treatment temperatures, chosen raw materials and the oxidation atmosphere.

CFs have been recognized as fibers that originate from filamentous carbon that is thickened by the Chemical Vapor Deposition (CVD) method. These micron size particles are produced using iron catalysts in a benzene or methane atmosphere mixed with hydrogen and can be dated back to early discoveries in the 1950s. On studying these Vapor Grown CFs (VGCFs) closely [49], it was found that nanometer sized filaments were being produced in abundance on the surface but were incorporated or submerged in the vapor deposited carbon.

A continuous fabrication process for these nanometer sized particles was introduced by Endo et al. [50] who proposed producing the fibers continuously and then wafting them out with the help of the gaseous production feedstock. After this, General Motors Research Laboratories published a process for continuous production of Vapor Grown Carbon Nanofibers (VGCNF) by using gaseous and liquid catalysts [51,52]. On a commercial scale, Applied Sciences Inc., in collaboration with General Motors Research, started marketing VGCNF with a stacked-up morphology and different surface-carbon-

deposition thickness in 1991. CNFs have two major fabrication methods: catalytic vapor deposition growth and electrospinning.

2.4.1.1. Synthesis of CNF

2.4.1.1.1. Preparation by electrospinning.

One of the methods of fabricating CNF is by electrospinning a polymer solution of CNF as shown in Fig 2.3. Polymer nanofibers are prepared as the precursor for the fabrication of CNFs using electrospinning. These polymer solutions and the processing conditions then decide the final properties of the CNF fabricated. Most commonly used polymers include PAN and pitches, but polyvinyl alcohol (PVA), polyimides (PIs) polyvinylidene fluoride, lignin and phenolic resins are also used [53]. After fabricating the polymer nanofibers, these are carbonized to form CNFs. The crystallinity, purity, diameters and the morphology of the CNFs is dependent on this heat treatment and the its parameters such as temperatures and pressures.

After carbonizing the polymer nanofibers, the nanofibers are then heated at 1000° C in a specific environment which causes a change in the volume and weight, usually resulting in a decrease of the CNF diameters. Inagaki [53] have made the CNF using this process and have classified the nanofibers as per their structure and properties. Also, Zhang et al. [54] talked about the preparation and applications of electrospun CNFs. Electrospun CNFs are prone to form webs or mat-like structures which make them useful as electrode materials for supercapacitors and batteries.

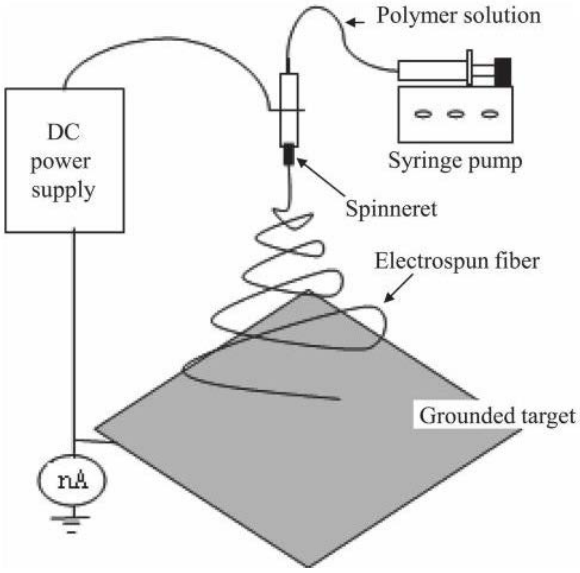

Fig 2.3: Schematic of the electrospinning setup for fabricating CNF [53].

2.4.1.1.2. Preparation by Catalytic Chemical Vapor Deposition Growth.

This method can be used to prepare two kinds of CNF, namely, cup-stacked CNF and platelet CNF. Ge and Sattler [55] first introduced the cup-stacked CNF (Fig.). The cup-stacked morphology of the nanofibers creates many reactive edges on the outside and inside of the nanofiber as shown in Fig. 2.4. These reactive edges can help with the effective dispersion and essential transfer of stress in the polymer matrix, after functionalization of these edges to interact with the matrix [56]. These open edges can also allow small molecules or ions to enter and intercalate between the graphene layers which creates an application of these nanofibers in fuel cells or lithium batteries as electrodes [57].

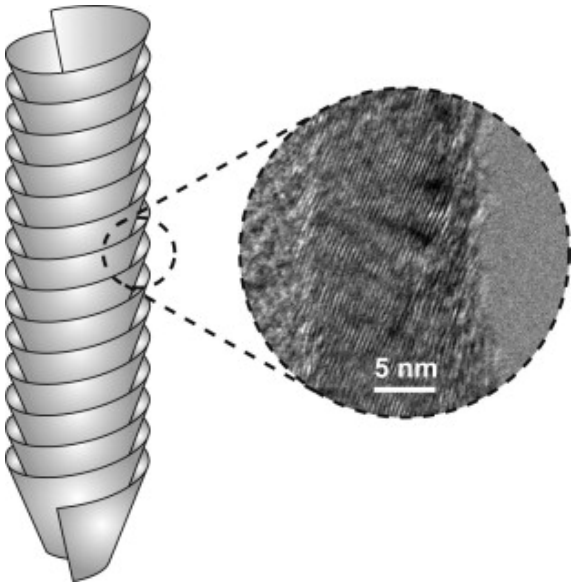

Fig 2.4: Cup-Stacked CNF [58].

Catalytic vapor deposition uses metals as catalysts that are capable of dissolving carbon to form metal carbides. Few examples of such metals are iron, cobalt, nickel, chromium and vanadium. For providing carbon for the reaction, methane, carbon monoxide, ethyne or ethene are used. The shape of the catalytic metal particles governs the shape of the structure of the CNFs. The deposition of the hydrocarbons dissolved in the metal particle and their precipitation on the metal surface as graphitic carbon has been the described growth mechanism [59].

2.4.1.1.3. Production of VGCNF

The process for production of VGCNF was introduced by Applied Sciences Inc., which involved the use of natural gas as the primary feedstock along with catalytic iron particles resulting from the decomposition of Fe(CO)5. In general, carbon monoxide or hydrocarbons including natural gas, acetylene, benzene, propane, etc. can be used along with catalytic metals such as Fe, Au, Co, Ni or metal alloys such as Fe-Ni and Ni-Cu

[60,61]. The decomposition of the hydrocarbons on the metal catalyst causes both the nucleation and growth of the nanofibers [62]. The process has been depicted in Fig. 2.5.

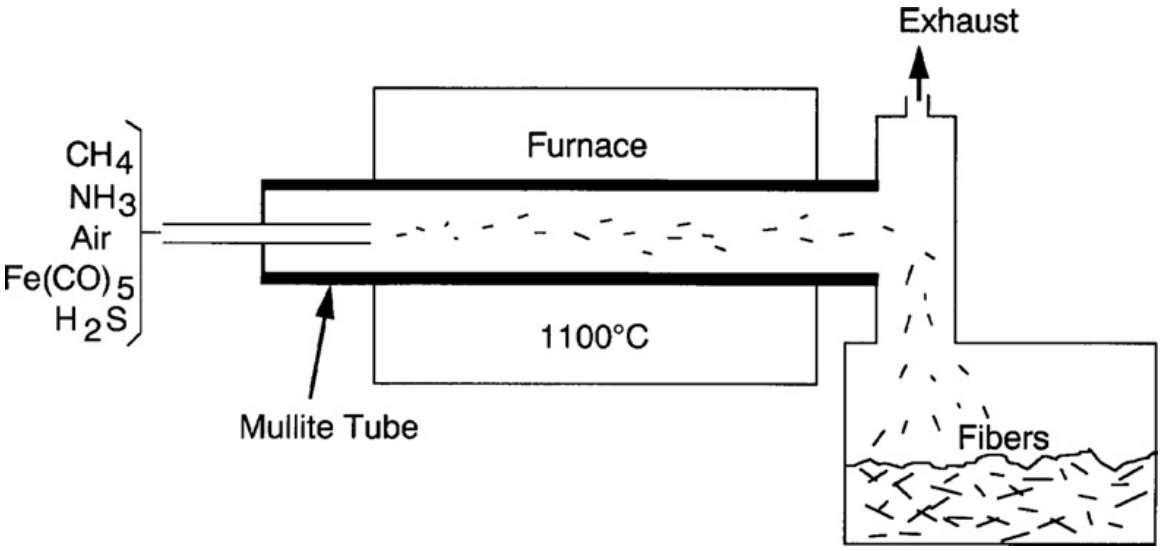

Fig. 2.5: Manufacturing apparatus for VGCNF [63].

Surface treatments of VGCNF are sometimes necessary to achieve adequate fiber-matrix adhesion. This adhesion is a crucial factor in manufacturing composites because if the adhesion is poor it might lead to a decrease in the properties of the nanocomposites. Some of the useful surface treatments include soaking in nitric/sulfuric acid mixtures, etching in air at ~400°C, or soaking in peracetic acid. Some of these treatments have been known to add oxygen equivalent to 1/4th of the fibers surface. In PP composites, although it was seen that a low amount of oxidation, 4% surface oxygen atoms, produced optimum tensile strength [64]. Oxygen concentrations above this tends to decrease the tensile properties, which can be attributed to the low surface energy of PP which makes it difficult to bond to highly oxygenated nanofibers. But in the case of epoxy, a highly

oxygenated nanofiber surface increased the strength by 25% and the modulus by 140% at 4 wt% loading level [65].

2.4.1.2. Properties and applications of CNFs

In this work, we will be mainly focusing on Vapor Grown CNF for which the properties and application have been explained in this section. CNF properties lie between those of CNTs and CFs. The tensile strength and tensile modulus of CNFs are around 2.92 GPa and 240 GPa respectively, while thermal conductivity and electrical resistivity lie around 1950 W/m K and 1×10^{-4} Ω cm, respectively [47,63,66,67].

The tensile properties of CNFs depend on the fiber diameter [68]. It has been seen that nanofibers 100 nm in diameter have a tensile strength of 2.2GPa, while those of 300 nm have a tensile strength of 1.77 GPa [48]. This can be because of a change in the morphology of the nanofibers with an increasing diameter or due to an increase in the defects in the nanofiber relative to an increase in the fiber diameter. The values for tensile strength and modulus mentioned above have not been directly measured but are used in the literature based on fibers 7.5 μm in diameter. The lower limit of tensile strength and modulus values for the most common VGCNF, the Pyrograf® III, have been estimated experimentally based on the mechanical properties of 15.5 vol% CNF reinforced epoxy. The tensile strength was found in the range of 1.7-3.38 GPa and the modulus was found in the range of 88-166 GPa [69].

The volume electrical conductivity of VGCNF was measured by Endo et al. [47] for nanofibers with diameter 100-200 nm and lengths 10-20 μm. carbonization at 1200°C decreased the volume resistivity of the fibers to 10^{-3} Ω cm, while graphitization reduced

it even further to 10^{-4} Ω cm. These CNFs have a higher resistivity as compared to CFs, which have resistivity of 6×10^{-5} Ω cm due to a lower crystallinity [47,67]. Electrical conductivity of VGCNFs has also been found to be catalyst and feedstock types dependent by Lee et al. [61]. Thermal conductivity for CNFs is 1950 W/m K, which is highest among any commercially available CFs but, when compared to MWNT and SWNT, which have thermal conductivity around 3000 W/m K and 6600 W/m K respectively, this value is very low [70–72].

Because of the properties mentioned above, CNFs have various application in different industries. In the automotive industry, CNFs can be utilized for lower costs, lower environmental emissions, better quality and less fuel consumption. These outcomes can be achieved by using CNFs for automotive electronics shielding, electrostatic painting for exterior panels, and also improvement of stiffness in tires by addition of CNFs [48]. CNFs can also be used as electrodes and support materials for batteries, where they seem to be better than metal oxides and sulfides in regards with thermal and chemical stability, cost, environmental impact and ease of formulations [47,73].

2.4.2. Carbon Nanotubes

Carbon Nanotubes, discovered in 1991, have since been gaining huge interest of researchers because of their exceptional chemical and physical properties. They display a combination of extraordinary thermal, mechanical and electrical properties. This makes them an excellent candidate as an advanced nanofiller material for composites. CNTs have been used by researchers to make electrically and thermally conductive plastics, exploiting the electrical and thermal conductivity of CNTs and their high aspect ratios

[74,75]. Using CNTs as reinforcements in polymers is probably the most promising area of research as the mechanical properties enhancement due to CNTs can be exceptional. Before CNTs, carbon in filler form has been used as mesoscale carbon fibers which have strength and stiffness in the range of 1.5-4.8 GPa and 230-725 GPa respectively [76]. But since the advent of nanotubes, they have become much more interesting to researchers. This is because comparable or better properties can be achieved using nanotubes as compared to mesoscale fibers, at much lower filler loading level.

2.4.2.1. Synthesis of CNTs

There are three main methods that are used for the synthesis of CNTs: Arch discharge, laser ablation and catalytic methods like chemical vapor deposition CVD [77]. Arc discharge and laser ablation are the methods that can provide high purity nanotubes, but a low yield, that is in grams. For more quantity, CVD is used which can be utilized for extended industrial production but the yield is with higher defect density.

2.4.2.1.1. Arc Discharge

This is the most common and easiest method to make CNTs. In this technique, CNTs are grown on graphite electrodes, in the presence of an inert gas such as helium or argon, during the direct current arc-discharge evaporation of carbon. This creates a plasma in between the cathode and the anode which has temperatures of approximately 3700-4000 °C [78]. This temperature makes the carbon on the anode to vaporize and deposit on the cathode.

2.4.2.1.2. Laser Ablation

In this method, a continuous laser is used for vaporizing a target that consists of graphite and metal catalysts (cobalt or nickel), in a 1200 °C furnace in the presence of an inert gas such as helium or argon [78]. As the vapors start to form, C3, C2, C and catalyst vapors are formed. When the vapors cool, carbon species with small molecular weight combine to form larger molecules. Catalysts help prevent the carbon from forming closed cage structures. Nanotubes keep on growing until there are too many catalyst atoms at the end of the nanotubes. This method gives a high yield of more than 70% of SWCNTs.

2.4.2.1.3. Chemical Vapor Deposition

Using this technique, massive quantities of nanotubes can be generated, while having the capability of controlling the growth direction on a substrate. In this, a hydrocarbon is decomposed in the presence of a catalyst. A mixture of hydrocarbon gas, methane or ethylene, acetylene and nitrogen are introduced in a reaction chamber. Due to the reaction, the decomposition of hydrocarbons at 700-900 °C and atmospheric pressure, forms nanotubes on the substrate.

CNTs can be categorized into Single-Walled Carbon Nanotubes (SWCNTs), Multi-Walled Carbon Nanotubes (MWCNTs) and Double-Walled Carbon Nanotubes (DWNTs). SWCNTs have very small diameters, close to 1 nm, but the length can be up to several thousands of magnitudes longer. They are conceptually a seamless cylinder of one-atom-thick layer of graphite, also called graphene. SWCNTs are more important than MWCNTs due to their important electrical properties. MWCNTs are multiple layers of graphite that together form a tubular structure. MWCNTs have a lower modulus and

tensile strength as compared to SWCNTs. They also have bigger diameters in the range of 10-100nm. Also, due to a larger cross-section they are more rigid than SWCNTs.

Nanotubes diameters range from 1-100 nm and they can have lengths of up to several millimeters [79]. They have low densities and superior Young's modulus values of up to 1 TPa [80]. Also, they have strengths measured up to 63 GPa which is much more than any other carbon fibers [81]. The reported tensile strength, modulus and Poisson's ratio for SWCNTs are in the range of 37-100 GPa, 640 GPa to 1-2 TPa [82], and 0.14-0.28 respectively [83]. This mean that the tensile strength is approximately up to 20 times more than that of graphite and the modulus can be up to 4 time more than that of graphite [78].

2.5. Conclusion

The literature review presented here has been utilized in this work to understand the results and to present the observations. The strain rate effect and the ultrasonication process have been explained along with some common carbon nanostructures and their nanocomposites to establish a background for the thesis. The next chapter talks about the processes used for the fabrication of the nanocomposites, the testing methods involved and the design of an injection mold crucial to this thesis.

CHAPTER III

DESIGN AND EXPERIMENTS

3.1 Introduction

To study the effect of addition of carbon nanofibers on the strain-rate dependency of the polymer and the various mechanical and thermal properties, several experiments were conducted. The experiments for mechanical properties include the tensile testing of pure PP, processed PP, and PP/CNF nanocomposites. To perform these tests, various design and experiment considerations were accounted for. Along with the mechanical properties, the effect of the processing and addition of carbon nanofibers on the thermal properties of the polymer were studied using TGA. This chapter talks about the equipment and materials that were used for the experimentation, design for injection molding, design of the apparatus for mixing PP/CNF nanocomposites and details of the testing of the mechanical and thermal properties for the polymer and its nanocomposite.

3.2 Injection Mold Design

3.2.1 Introduction

An injection mold was designed for producing tensile test specimens, to test the mechanical properties of the pure polymer as well as fiber filled polymers. The design of the tensile test specimens that would be produced by injection molding was based on ASTM standards. ASTM D638-14 has been used to define the dimensions for the tensile test specimens. ASTM D638 is a test method for plastic materials that helps produce tensile property data for their control and specification [84]. This test helps in determining the tensile properties of reinforced and unreinforced plastics by using

standard dumbbell shaped test specimens. The conditions for pretreatment, temperature, humidity and testing machine speed are pre-defined in the standards. As per these standards, all samples must be prepared in the same way and there should be uniformity amongst samples. Therefore, for the convenience of the work, the injection mold had to be a multi-cavity mold to have consistency in the tensile test specimens, to achieve consistent results in testing. Based on the capacity of our injection molding machine, we considered using ASTM D638-14 Type V as the standard dimensions for the specimens.

The thickness for injection molded specimens has been specified as 3.30 mm in the ASTM standards, which has been used in our mold. The dimensions for the sample are the same as provided in the standards, which have been highlighted in the Fig 3.1. A typical sample based on the ASTM standards has been presented in Fig. 3.2. Using these dimensions and keeping in mind the capacity of our injection molding machine, a multi-cavity mold had to be designed that contains the maximum cavities possible and a balanced design. In the next section, the procedure for designing the multi-cavity mold has been explained.

Specimen Dimensions for Thickness, *T*, mm (in.)[A]

Dimensions (see drawings)	7 (0.28) or under		Over 7 to 14 (0.28 to 0.55), incl	4 (0.16) or under		Tolerances
	Type I	Type II	Type III	Type IV[B]	Type V[C,D]	
W—Width of narrow section[E,F]	13 (0.50)	6 (0.25)	19 (0.75)	6 (0.25)	3.18 (0.125)	±0.5 (±0.02)[B,C]
L—Length of narrow section	57 (2.25)	57 (2.25)	57 (2.25)	33 (1.30)	9.53 (0.375)	±0.5 (±0.02)[C]
WO—Width overall, min[G]	19 (0.75)	19 (0.75)	29 (1.13)	19 (0.75)	...	+ 6.4 (+ 0.25)
WO—Width overall, min[G]	...	...	...	...	9.53 (0.375)	+ 3.18 (+ 0.125)
LO—Length overall, min[H]	165 (6.5)	183 (7.2)	246 (9.7)	115 (4.5)	63.5 (2.5)	no max (no max)
G—Gage length[I]	50 (2.00)	50 (2.00)	50 (2.00)	...	7.62 (0.300)	±0.25 (±0.010)[C]
G—Gage length[I]	...	...	...	25 (1.00)	...	±0.13 (±0.005)
D—Distance between grips	115 (4.5)	135 (5.3)	115 (4.5)	65 (2.5)[J]	25.4 (1.0)	±5 (±0.2)
R—Radius of fillet	76 (3.00)	76 (3.00)	76 (3.00)	14 (0.56)	12.7 (0.5)	±1 (±0.04)[C]
RO—Outer radius (Type IV)	...	...	...	25 (1.00)	...	±1 (±0.04)

Fig 3.1: Specimen Dimensions from ASTM D638-14 [84].

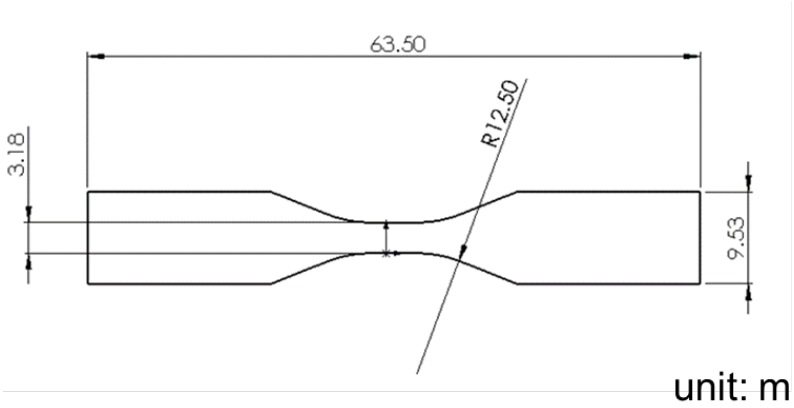

Fig 3.2: Dimensions in mm for D638 Type V.

3.2.2 Design Considerations

Injection mold designs have several constraints to follow, and the first of them is the limit in the specifications of the machine. The injection molding machine used in this research was the BMI-SHOOTER, Model 150a Plastic Injection Machine purchased from LNS technologies. It is a manually operated desktop injection molding machine with a shot capacity of 20.5 cc. The important specifications including the shot capacity, maximum size of the mold and the temperature ranges that the machine can withstand have been mentioned in Table 3.1.

Specification	Values
Maximum Shot Capacity	20.5 cc (PS)
Maximum Mold Dimensions	203.2 mm W X 127 mm H X 127 mm D
Temperature Range	Room Temp - ~255° C

Table 3.1: Specifications of the Injection Molding Machine.

These specifications provided by the equipment manufacturer have been strictly adhered to in this work. The shot capacity for the machine is provided by the manufacturer based on polystyrene (PS), which must be converted into the shot capacity for the particular material that will be used in the research. For our research, we will be using PP. The shot capacity for PP based on the shot capacity for PS can be calculated by:

$$\text{Shot capacity for PP} = \frac{\textit{Specific Gravity of PP}}{\textit{Specific Gravity of PS}} \times \text{Shot capacity for PS}$$

$$= \frac{0.9}{1.04} \times 20.5 \text{ cc} = 17.74 \text{ cc}$$

Therefore, a maximum of 17.74 cc PP could be injected using our machine in one shot. According to general injection molding guidelines, a general thumb rule of 50% shot size exists. According to this rule the shot that needs to be injected in the mold should be around 50% of the total shot capacity of the machine. In general, the shot size can range from 20% to 80% of the barrel capacity of the machine, based on the heat sensitivity of the material. This guideline has also been taken into consideration while making the design for the multi-cavity mold. One tensile test specimen, with dimensions the same as provided in ASTM D638 Type V, has a volume of 1.57 cc. Also, the runners and the sprue for the mold need to be taken into consideration. Considering the 50% shot size rule and runner balancing, a 4-cavity mold was decided to be made.

Another thing that needed to be considered for designing the runners and gates in the mold was injection pressure. As our machine is a handheld machine, therefore the pressures applied are relatively much lower than the pressures available on commercial

injection molding machines. Using the dimensions of the lever and the ram head of the barrel, calculations were made for the maximum injection pressures that we would be able to apply. The mechanical advantage provided by the lever increases the 881 N force applied to 6682.16 N. Then using the surface area of the injection ram, the maximum injection pressure comes out to be 23.5 MPa. This injection pressure was considered while designing the gates and the runners of the injection mold and was also used in the simulation of the mold designs. As the machine is manually operated, the pressure variations due to human error have been accounted for using different pressure values in the simulations which have yielded the same results, thus confirming no effects of the pressure variations on the samples. A few designs were considered for the 4-cavity mold out of which two designs were finalized for further analysis and simulations, which have been explained in the next sections.

3.2.3 Multi-cavity Mold designs (4 cavities)

The two finalized designs on which simulations were performed have been shown in Fig 3.3. These designs were made using SolidWorks, considering all the injection mold design guidelines. The cavities were made first, along with the runners and sprue for volume measurements and ease of designs. The cavities were also needed for simulation in the Moldex 3D software. The molds were then modeled by carving the designs of the cavities into solid cuboids for efficient designing. Initially a 3-part mold was to be made for easy removal of the part after injection molding, but as the design progressed and changes were made in the models, a 2-part mold was considered a better option. This was

because the runners and sprue could be designed much more efficiently in a 2-part mold design.

3.2.3.1 Design 1:

As shown in Fig. 3.3(a), the first design was made with the 4 tensile bars on one side of the main runner of the injection mold. The mold for this cavity was made within the maximum dimensions specified by the machine and also the total cavity volume including the runners and sprue is 10.16 cc which is more the 50% shot size range. All the four secondary runners are identical and the gates have been made large because of the pressure considerations explained above. All corners have been rounded for a better flow of the polymer and to avoid areas of stress concentrations inside the mold.

3.2.3.2 Design 2

The second design, as can be seen in Fig 3.3(b), is a more balanced design that was made with two tensile bars on each side of the main runner. This helps in making the polymer melt reach the cavities at the same time. The total cavity volume including the runners and sprue is 7.53 cc which is less than the 50% shot size range This design had many variations in the primary and secondary runner diameter and secondary runner lengths. A statistical analysis has been conducted to decide the runner lengths and diameter, which has been explained in later sections. The variations helped study the flow characteristics and also helped in controlling the outcome of the injection molding process. The design in the Fig 3.3(b) is a SolidWorks model of the final design that was decided upon after a set of simulations and analysis.

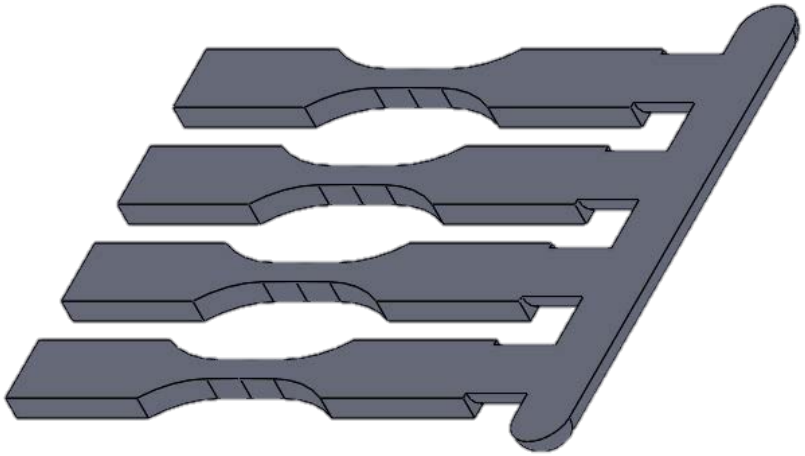

(a)

(b)

Fig 3.3: Design of Injection mold cavity, a) Design 1, b) Design 2.

3.2.4 Design Geometry Simulations

Several simulations were conducted on the two designs that were decided upon. These simulations were conducted using Moldex 3D to check the melt flow in the mold and also to check for any complications that might arise in the molded part because of the geometry. Moldex 3D was used for injection molding simulations conducted in this research. It is capable of simulating the polymer melt flow inside the injection mold, while allowing for variation in hundreds of injection-molding parameters and providing knowledge about several outcomes in the injection molding process. Various parameters like injection pressure, injection times, injection temperatures, mold temperatures,

packing time, cooling time, and many more can be controlled. Also, outcomes such as shear rates, molded in stress, melt filling, viscosity, and many more can be analyzed to improve the injection molding process being done.

Moldex 3D helped this research by modeling how the polymer is flowing. One of the major outcomes that was considered for the analysis in this research was shear rates. Shear rate is the rate of shear deformation of the material during the processing of the polymer. High shear rates may drastically deform the molecular chains and may even cause them to break. This can weaken the strength of the product. As the product, here is a tensile testing specimen for testing of the material properties, the molecular chains must stay intact so as to have a better idea of the properties of the material.

For deciding on which geometry is better, a hypothesis test was conducted for the two designs. The hypotheses test considered one of the material property that is part of the vast database present in Moldex 3D which tells a whole list of properties for a great amount of material from different manufacturers. The property chosen for hypothesis testing was Melt Flow Index (MFI). MFI values were taken from 5 different material suppliers of PP using the Moldex 3D material bank. MFI was chosen as the property for comparison because it is inversely proportional to the viscosity of the material. As the viscosity increases, the melt flow index decreases. Also, viscosity is in turn inversely proportional to the shear rates. Thus, using this indirect relation, MFI was chosen as the appropriate property. The MFI values for the chosen materials are also listed in the table below. The materials were chosen based on similar MFI values so as to not vary the shear rate vales by massive amounts. In Table 3.2, the company name, the product chosen, MFI

of the material and the shear rate values obtained from simulations of both the designs has been listed.

Company Name	Product Name	MFI (g/10min)	Shear rate (Design 1) (/sec)	Shear rate (Design 2) (/sec)
Noble Polymers	FORTE 18CPP091	17	3555.36	1263.93
Ginar	APLAX P0413GN	18	3111.79	1394.49
LCY Chemical	Globalene PT331M	15	2492.3	1423.61
Prime	PRIME POLYPRO J-106G	15	2846.05	1371.87
Sabic	PP 576P	19	3428.36	1434.02
		Mean	3086.772	1377.584

Table 3.2: Materials and shear rate values for comparison of designs.

The simulation done using Noble Polymers PP have been presented in Fig 3.4 for comparison. The simulation clearly shows the major difference between the two designs. Design 1 is an unbalanced design because of the absence of any shear rate in the middle two samples, whereas the outer two samples have relatively high shear rates in the gage section. Design 2, on the other hand, is much better balanced in terms of shear rate distributions and visibly all the samples seem to have the same effect on their molecular chains. Also, the shear rate magnitude is much lower in the case of Design 2, because of being a balanced design.

A two-sided T-test (hypotheses test) is done using Minitab software for design 1 and design 2. The hypotheses are as follows:

H_0: The two geometries are same. i.e. H0: $\mu_1 - \mu_2 = 0$

H_A: The two geometries are different. i.e. HA: $\mu_1 - \mu_2 \neq 0$

Here, μ_1 is the mean value of shear rates obtained using PP products from different manufacturers in Design 1. And μ_2 is the mean value of shear rates obtained using PP products from different manufacturers in Design 2.

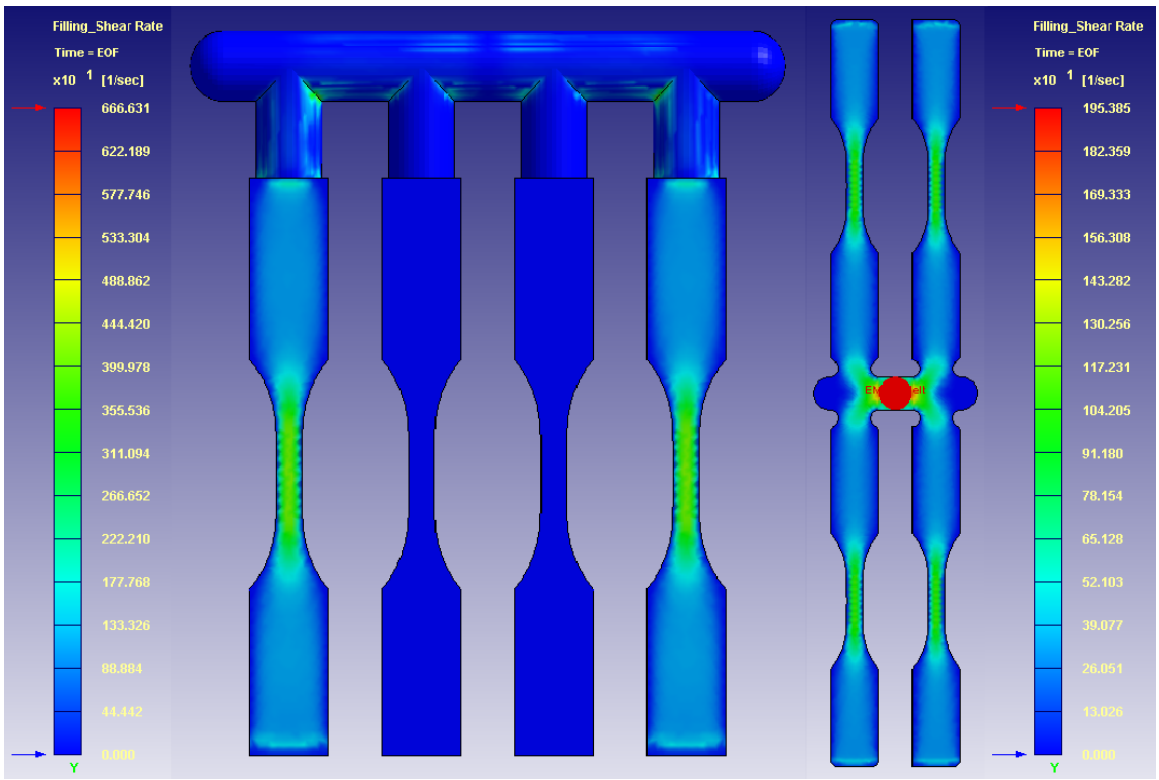

Fig 3.4 Comparison of the shear rate values obtained from Moldex 3D for design 1 (left) and design 2 (right) using Noble Polymers PP.

The p-value obtained from the T-test was 0.001. Considering this p-value, the null hypotheses can be rejected and it can be stated that the two geometries are different. As it is a two-sided test, it can also be said that the second design is better than the first, due to its low shear rate values which has been attained through a balanced design, although

further investigation can be done for those purposes. Therefore, design 2 was used as the suitable design for the injection mold.

Study of Runner diameter and length

As stated earlier, runner geometry is important for proper filling of the cavities and also in a balanced manner. After finalizing the multi cavity design, a study was done for determining dimensions of the runner to minimize the shear rates. To choose the appropriate runner diameter and length an analysis of variance (ANOVA) was performed with these two as independent variables. Two values of runner diameter, such as 6.35 mm and 7.9375 mm were chosen because the runner needs to be wide for proper flow of melt as the injection pressures for our injection molding machine are quite less as compared to a conventional molding machine. Also, two values of runner lengths 6.35 mm and 12. 7 mm were chosen, considering the geometry restrictions to clamp the mold in the injection molding machine. The two geometric parameters, such as the length and diameter of the runners were considered as two factors whereas the shear rate is a dependent variable. The purpose of this study is to decide the dimensions that allow the smallest shear rate within the considered range of levels for the two factors. Table 3.3 shows the selected factors and levels for this study.

The simulation results for 6.35 mm diameter and length, and for 6.35 mm diameter and 12.7 mm length have been presented in Fig. 3.6. The simulation results have a difference in the shear rates due to change in the geometry of the runners as can be seen in Table 3.3. An ANOVA was performed using Minitab and the results have been show in Fig. 3.5

Runner Diameter (mm)	Runner Length (mm)	Shear Rate (s^{-1})
7.9375	12.7	1275.67
6.35	6.35	1175.13
7.9375	6.35	1193.80
6.35	12.7	1263.93

Table 3.3: Factors and levels of runner length and diameter.

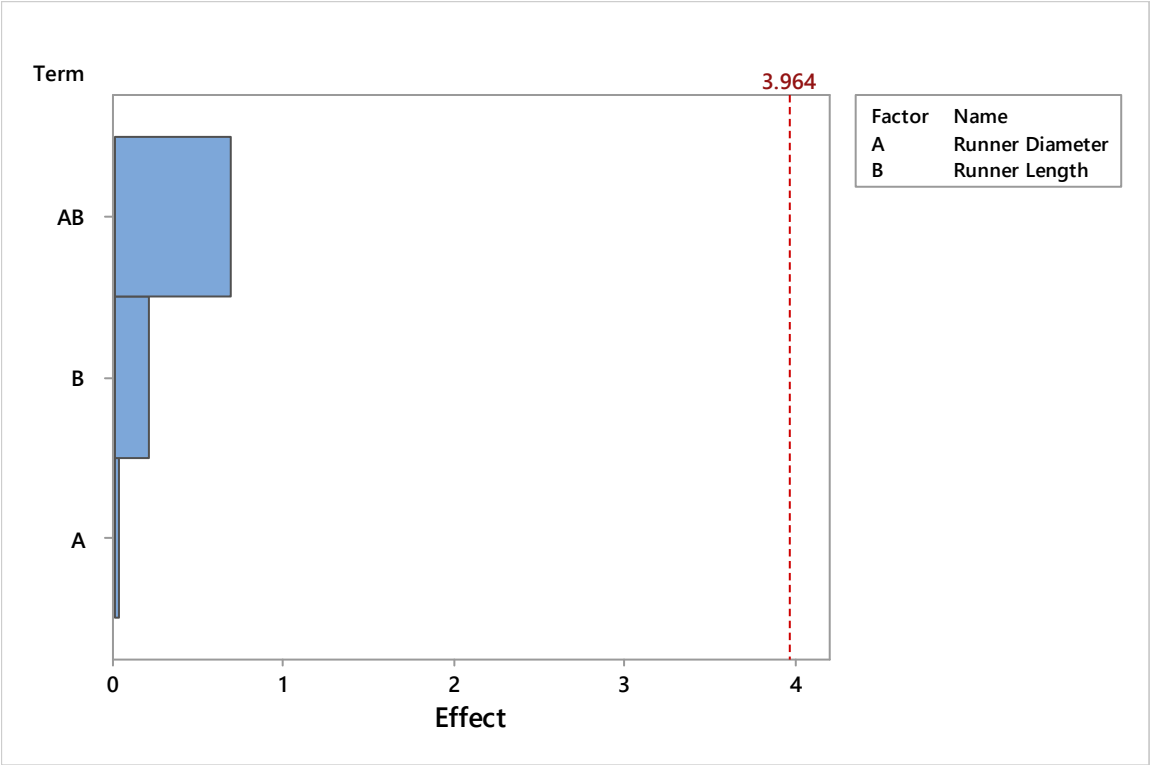

Fig 3.5: Pareto chart for shear rate analysis at 0.5 level of significance using ANOVA

From the ANOVA, it was seen that there is no significant variable obtained from the study. Although, it could be seen from the analysis that as the runner diameter and length increase, the shear rate increases. For these reasons, a short runner diameter and runner length were chosen. Using the results obtained a runner diameter of 6.35 mm and

runner length of 6.35 mm were chosen as the dimensions for the runner design to help minimize the shear rates in the tensile bars produced. The sprue length was taken as 25.4 mm to have better flow characteristics and to ease the flow of the polymer melt.

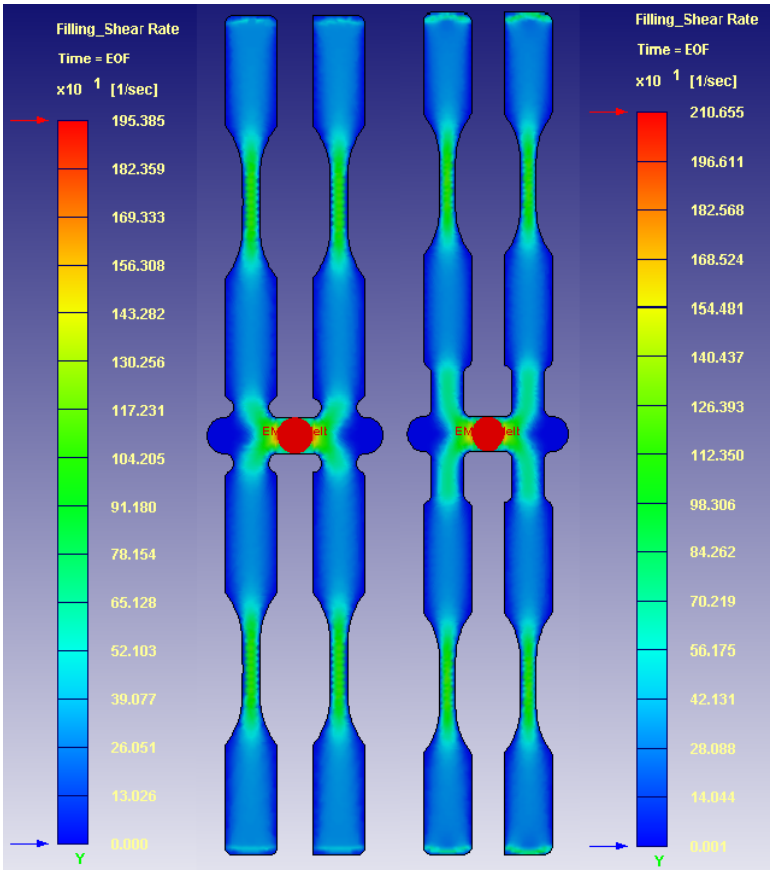

Fig 3.6**:** Shear rate simulation for 6.35 mm diameter and length samples (left) and for 6.35 mm diameter and 12.7 mm length samples (right).

3.2.5 Final mold design

The final mold design based on all the statistical analysis is shown in Fig. 3.7. This design helps keep the polymer flow balanced and reduces the shear rate in the polymer melt. The parts produced thus have less effected mechanical properties, which need to be tested. The top part of the mold contains an inlet nozzle based on the nozzle

dimensions of the injection molding machine. To avoid flashing and to secure the two parts together, fasteners were used in the mold. The tensile test results and analysis will be seen in subsequent chapters. The final mold was manufactured out of aluminum alloy 6061 by Protolabs.

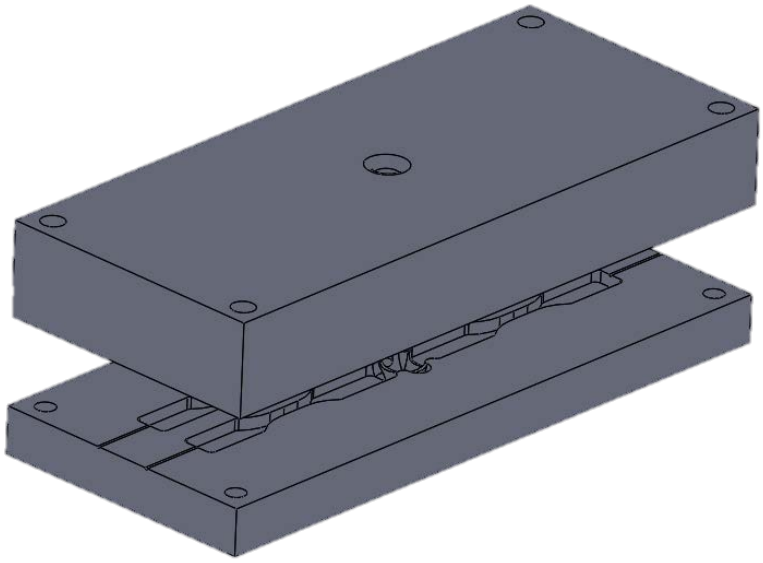

Fig 3.7: Injection mold Part A (top), Part B (bottom).

3.3 Nanocomposite Fabrication Methods

In this research, PP/CNF nanocomposites have been made using the ultrasonication process for dispersing the carbon nanofibers into the polymer matrix. PP used in this research was acquired from LNS technologies, which is a commercial grade polymer that has 10% mineral filler composition. PP was dissolved in o-xylene (99.0%) obtained from Alfa-Aesar for nanocomposites preparation. Along with the ultrasonication process, another process has been used in the experiments which utilizes mechanical mixing, using a magnetic stir bar for dispersing the nanofibers into the polymer matrix. The details for these processes have been provided in the sections below.

3.3.1 Fabrication of Nanocomposites using Ultrasonic-Assisted Mixing

Ultrasonication, as explained in Chapter 1, has been used for the dispersion and distribution of nanofibers in the polymer matrix. CNF with a diameter of 150 nm and a length of 6 µm (CM-150) obtained from Hanwha Chemical, South Korea have been used as the nanomaterials that are dispersed in the PP matrix by dissolving PP in xylene and dispersing the nanofibers using ultrasonication. An ultrasonic horn made out of Ti_6Al_4V alloy has been used for providing the ultrasound to the solution that is externally heated to help initiate dissolving of PP pellets into xylene.

As the processing cell geometry is a crucial factor for ultrasonication, the processing cell has been designed and fabricated in the lab using borosilicate glass. The geometry is based on the previous work done at CAMMP lab by Pasumarthi et al. [85] for determining the geometrical parameters for the ultrasonication processing vessel to have effective ultrasound effects on the solution. The setup and the processing cell have been shown in Fig. 3.8.

The process involves introduction of PP pellets into xylene in a ratio of 1:10. Xylene is present in the specially designed processing vessel which is pre-heated to 100° C before introducing the PP pellets. After the feeding of PP into the processing cell, ultrasonication is turned on at 50% amplitude and 0.5 wt% CNF are added slowly to the processing cell. The sonicator horn immersion depth into the processing cell has also been decided based on the work of Pasumarthi et al. [85]. This process is done for 30 minutes with constant heat being supplied to the processing cell at 100° C.

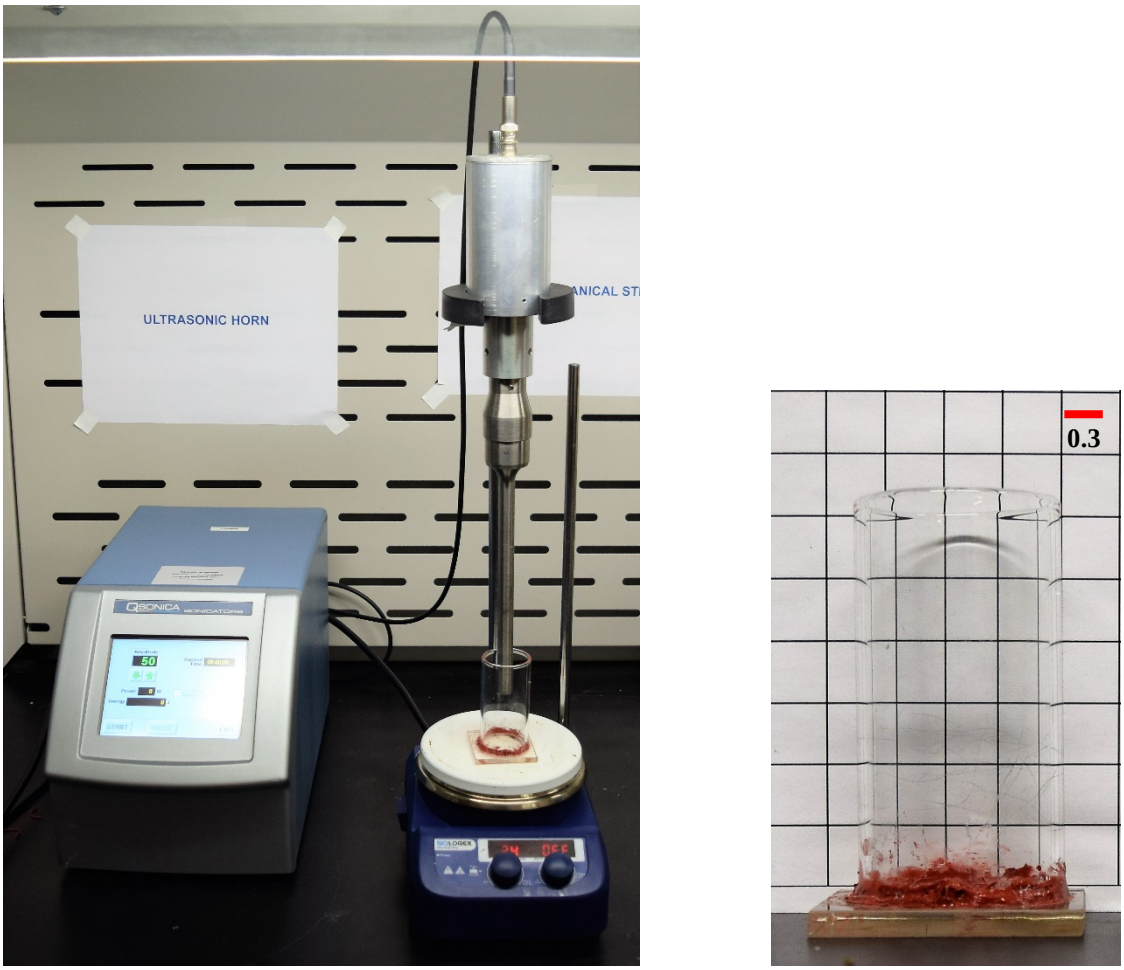

Fig. 3.8: Setup for ultrasonic-assisted mixing (left) and the processing vessel used (right).

Ultrasound by itself can disperse the carbon nanofibers throughout the matrix but once the ultrasonication processing is turned off, the nanofibers might agglomerate again. To avoid this, after finishing the ultrasonication process, the solution is added to cold water to help the solution solidify easily and stop the movement of nanofibers in the matrix [86]. This solution, along with water, is then evaporated under a fume hood at 100° C for 48 hours. These nanocomposites are then transformed into tensile test specimens. The same processing was also done without the addition of nanofibers to understand the effect of processing on the polymer.

3.3.2 Fabrication of nanocomposites using mechanical mixing

Another method employed in this research for fabricating the nanocomposites is by mechanical mixing using a magnetic stir bar. The use of mechanical mixing for dispersing nanofibers in the Polypropylene matrix is an already established process [86,87]. This process has been used in this research to provide a comparison for the nanocomposites made by ultrasonic-assisted mixing process. The setup for the process has been shown in Fig. 3.9.

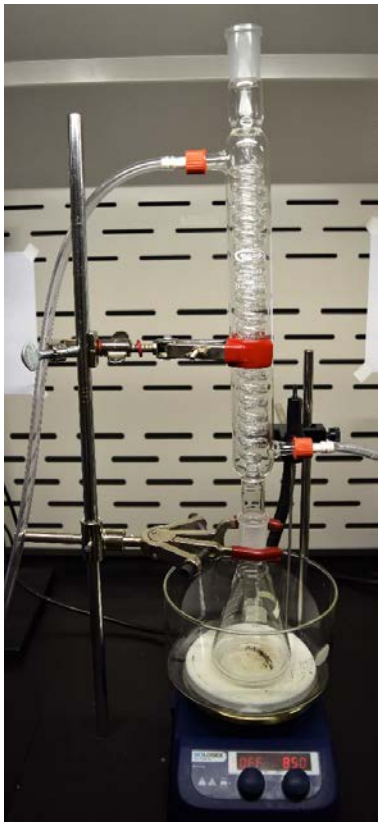

Fig. 3.9: Setup for mechanical mixing process.

In this process, PP pellets are added to pre-heated xylene in the ratio of 1:10. Xylene is pre-heated to 140° C to assist with dissolving of pellets as it is close to the boiling temperature of xylene. After feeding PP pellets, 0.5 wt% CNF are slowly added to the

solution. The solution is stirred at 850 RPM for 2 hours for dissolving PP and dispersing CNF in the matrix. After this the solution is then transferred to icy water and then evaporated in a fume hood at 100° C for 48 hours. These nanocomposites are then also used for making tensile test specimens. The same processing was also done without the addition of nanofibers to understand the effect of processing on the polymer.

3.4 Tests for Mechanical and Thermal properties

3.4.1 Tensile Properties Testing

Using the injection mold designed above, tensile test specimens were created by injection molding using pure PP pellets, dissolved PP pellets that were dissolved using ultrasonication and mechanical mixing, and nanocomposites. These samples were then used for testing the tensile properties. The tests were conducted on the computerized Instron Model 1125 universal testing machine at several quasi-static speeds ranging from 10^{-4} to 10^{-1} s^{-1}, to determine the strain rate dependent behavior of PP. For each strain rate, data have been obtained using a minimum of 4 standard ASTM tensile test specimens, manufactured from the same mold. The test results have been mentioned in Chapter 4 with a detailed analysis about the results. The distinct types of samples have been abbreviated for convenience as follows:

- Pure Polypropylene Samples: PP1
- Mechanically Mixed Dissolved Polypropylene Samples: PP2
- Ultrasonically Mixed Dissolved Polypropylene Samples: PP3
- Mechanically Mixed PP/CNF Nanocomposites: PPNC1
- Ultrasonically Mixed PP/CNF Nanocomposites: PPNC2

3.4.2. Thermal Behavior and Chemical Structure

The thermal behavior of the pure, the processed polymer, and its nanocomposites have been studied using a TGA Q5000 IR (TA instruments). The samples ranging between 5-15 mg and were heated from room temperature to 550°C at a heat rate of 10°C/min. The samples were heated in a nitrogen atmosphere with a gas flow rate of 50 cc/min. The results for TGA have been presented using three parameters, the initial degradation temperature, the onset temperature and the maximum of derivative TGA (DTGA) [88–90]. These parameters have been used to study the effect on the thermal stability by the processing and the addition of carbon nanofibers to the polymer. In order to study the chemical structures, FTIR was also used with a sample taken from the tensile test specimens. The FTIR was conducted on a Magna-IR spectrometer from Nicolet. They were collected from 4000 to 525 cm^{-1} at a resolution of 4 cm^{-1} over 16 scans.

CHAPTER IV

RESULTS AND DISCUSSIONS

4.1. Introduction

The results for the mechanical properties and thermal behavior of the polymer and its nanocomposites have been discussed in this chapter. This discussion has been divided into three sections. The first section talks about the results of the mechanical properties and thermal behaviors of the processed polymer, based on the different processes that were used for fabricating the nanocomposites, such as mechanical mixing and ultrasound-assisted mixing. The second section then talks about the effect of the addition of CNF to the polymer, on the mechanical properties and thermal behavior, based on the results from the tensile tests and the TGA. The last section talks about the effect of varying strain rates on distinct stages of the polymer, i.e. pure PP, the ultrasound-assisted dissolved PP, and the PP/CNF nanocomposites using strain rates varying from 10^{-4} s^{-1} to 10^{-1} s^{-1}.

4.2. Effect of processing techniques on Polypropylene

4.2.1. Mechanical Properties

This section talks about the effect of the processes on the mechanical properties of the material based on the tensile tests conducted at 10^{-2} s^{-1} strain rate. This strain rate has been recommended by the ASTM [84] standards for understanding the basic properties of a thermoplastic polymer. The results for the tensile tests have been shown in Fig. 4.1. in a stress-strain curve. As can be seen in Fig 4.1, there is a difference in the strength and ductility values of the pure (PP1) and the processed (PP2 and PP3) polymer.

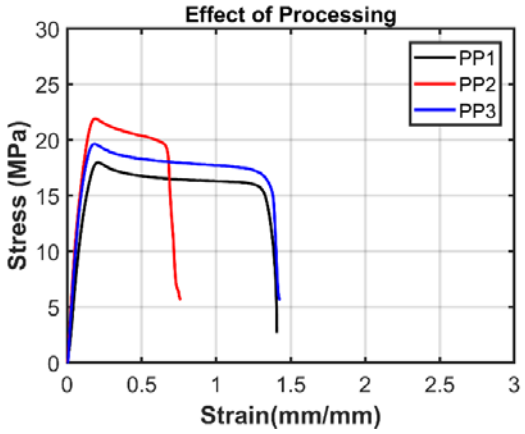

Fig 4.1: Stress-Strain curves for pure (PP1), mechanically (PP2) and ultrasonically (PP3) dissolved polymer at 10^{-2} s^{-1} strain rate.

The tensile strength of the processed polymers has increased as compared to the pure polymer as shown in the curves. This can be the result of an enhanced dispersion of the mineral filler that is present the polymer matrix, due to an additional mixing step. The mineral filler present, calcium carbonate, is commonly added to PP as a reinforcing agent to enhance the mechanical properties like tensile strength and toughness [91]. The presence of calcium carbonate has been verified using FTIR for the residue from the TGA performed on the samples. The FTIR results have been shown in Fig. 4.2. The peaks observed at 1795 cm^{-1}, 1412 cm^{-1}, and 875 cm^{-1} verify the presence of calcium carbonate. Calcium carbonate fillers could be treated with acrylic acid to enhance the dispersion of the filler in the polymer matrix and increase the bonding of the filler to the polymer matrix [92]. As a result of the surface treatment, calcium acrylate is formed that creates an enhanced bonding layer between the filler and the polymer matrix. Xylene that is a good solvent for calcium acrylate [93], has been used in this work for dissolving the polymer. Thus, calcium acrylate can be dissolved as a result of the processing, which can

affect the bonding capabilities of the filler and can also lead to agglomeration of the filler. The agglomeration of the filler in turn can lead to a reduction in the ductility as can be seen in the stress-strain curve for the mechanically mixed dissolved polymer (PP2).

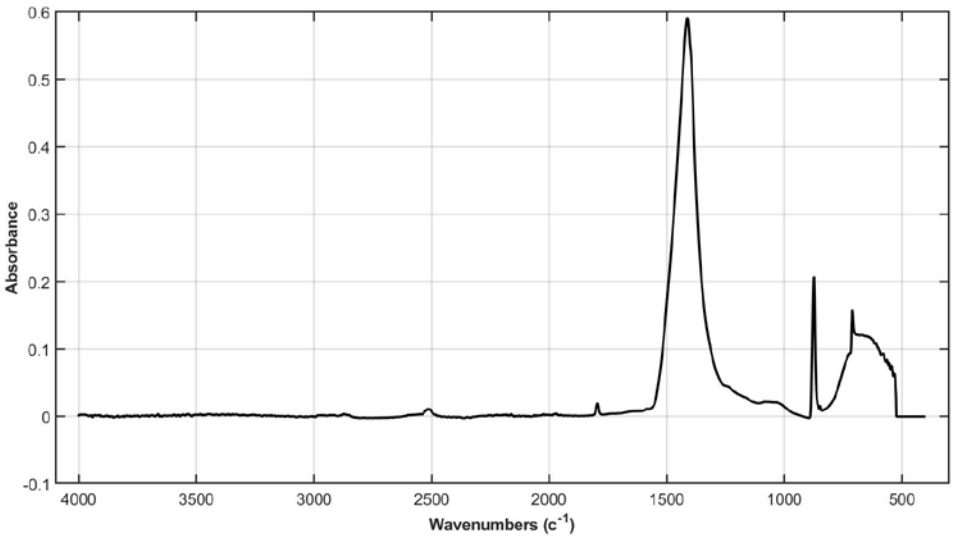

Fig. 4.2: FTIR results for TGA residue for verification of calcium carbonate.

The decrease in the tensile strength of the polymer processed through ultrasonication processing, as compared to the mechanical mixing process, can be attributed to the degradation of the polymer that is caused by ultrasonication. As mentioned before, ultrasonication can cause scission in long polymer chains and thus reduce the molecular weight of the polymer [36]. This degradation of the long polymer chains is the reason for the slight decrease in the tensile strength as compared to the mechanically mixed polymer.

On the other hand, the retention of ductility in case of ultrasonication is an interesting fact. One of the possible reasons is a better dispersion of the mineral filler caused by ultrasonication as compared to mechanical mixing. In addition, as the acrylate

coating is lost to xylene, another reason for the retention of ductility could be due to the attraction of the mineral fillers to the free radicals formed as a result of the chain scission of PP by the ultrasonication process [16,37]. When ultrasonication processing is done for a while, these free radicals can cause polymerization reactions in the solution. Polymerization reactions in the presence of the calcium carbonate fillers can lead to a good bonding of the filler with the polymer. This could mean that, even after losing calcium acrylate, calcium carbonate could still have good bonding with the polymer matrix because of the additional bonding with the free radicals, which would lead to an increase in the ductility, as compared to mechanically mixed dissolved polymer. As calcium carbonate has a characteristic of increasing the toughness in PP, a retention of the ductility of the polymer could be seen even after polymer degradation and the loss of calcium acrylate to xylene. As compared to mechanically mixed dissolved sample, ultrasonically processed polymer thus has a lower tensile strength but the ductility of the original polymer was retained. As the effect of polymer degradation caused by ultrasonication is combined with other reactions, the overall effect of ultrasonication on polymer degradation, although couldn't be ignored, was not very drastic.

4.2.2. Thermal Behavior

The effects of processing on the thermal behavior of the sample were studied using TGA. Fig 4.3 shows a comparison of the TGA curves for pure and the processed samples. The initial degradation temperature (T_{int1}) has been measured at 1% wt. loss of the polymer during the TGA. The onset temperature (T_{onset}) has been defined as the point of interception of the extension of the predegradation portion with the tangent to the

steepest portion of the mass curve during degradation[88–90]. The maximum temperature of derivative TGA (T_{max}) is defined at the maximum of the loss weight rate. As can be seen from the curves, the thermal stability of the polymer has decreased after processing. The degradation onset temperature, T_{onset} has decreased from 460° C for the pure polymer to 447°C for the mechanically mixed dissolved and 444°C for the ultrasonically mixed dissolved samples. All of the values for the TGA have been stated in Table 4.1.

The ultrasonication of the polymer solution has not caused a significant change in the thermal behavior of the polymer as compared to the mechanically mixed dissolved sample. The degradation temperature values for both mechanically mixed and ultrasonically mixed dissolved samples are very close and can be used to conclude that the effect of polymer degradation caused by ultrasonication is not seen as compared to the mechanical mixing process. As compared to the pure polymer, both the processes can be seen to cause a decrease in the thermal stability of the polymer by about 3%. This could be due to the shearing of the polymer chains during the processing that has resulted in a decrease of the chain entanglements in the molecular chains which would result in a less restricted movement of the molecules and thus a lower degradation temperature.

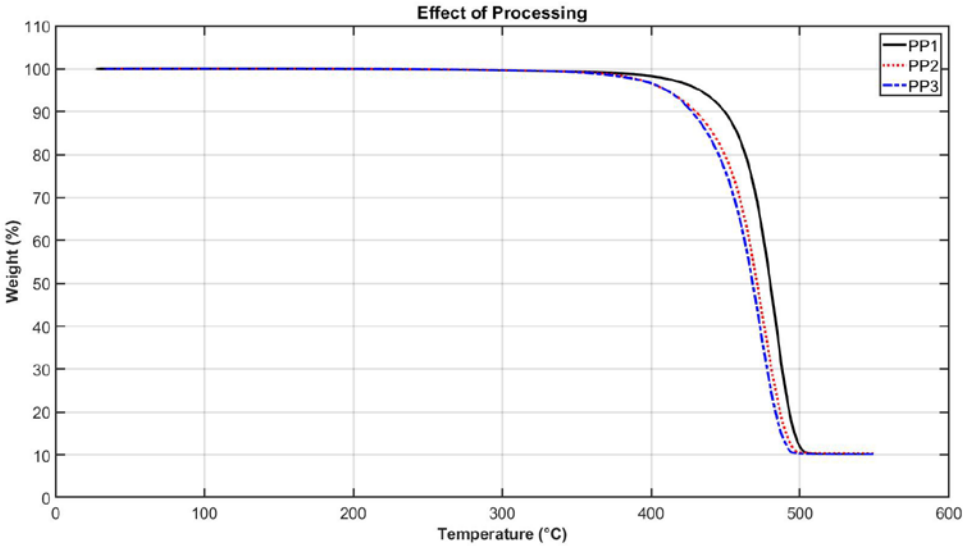

Fig. 4.3: TGA curves for pure (PP1), mechanically (PP2) and ultrasonically (PP3) dissolved polymer.

	T_{int1} (°C)	T_{onset} (°C)	T_{max} (°C)
PP1	375	460	483
PP2	363	447	474
PP3	358	444	473

Table 4.1: TGA results for pure polymer (PP1), processed polymer (PP2, PP3) and nanocomposites (PPNC1, PPNC2).

4.3. Effect of addition of carbon nanofibers to the polypropylene matrix

Using the ultrasonication processes mentioned above, PP/CNF nanocomposites were fabricated with 0.5 wt.% of CNF. CNF have been added to the polymer to understand the effect on the strain rate dependency of the polymer with the nanofibers addition. The effect on the strain rate sensitivity will be studied in the next section. This section talks about the change in the mechanical properties and thermal behavior of the polymer with the addition of nanofibers.

4.3.1. Mechanical Properties

The mechanical properties of the polymer have been studied using the tensile tests conducted at the fixed strain rate of 10^{-2} s^{-1}. Four samples of both the processed polymer and the nanocomposites were tested at this strain rate to understand the effect of the addition of nanofibers on the tensile properties, including tensile strength and ductility. The stress strain curves for the processed pure polymer (PP3) and the nanocomposite (PPNC2) have been presented in Fig 4.4. As it can be seen from the curves presented in Fig. 4.4, there was not a major effect seen on the mechanical properties of the polymer.

The most important reason that can be discerned is the less amount of carbon nanofibers that have been added to the polymer matrix. Although it has been reported that the addition of 0.5 wt.% has led to a more visible increase of the tensile strength and a decrease in the ductility [94,95], the nanocomposites in this study have been manufactured by different processes and as we have seen an effect of the processing presented above, it is not feasible to compare these results with the other works using different processes. With the addition of CNF to PP, there is an usual increase in the

tensile strength and a decrease in the ductility [94–97], which can also be seen minutely in this work. At higher strain rates, as will be discussed below, the effect of addition of CNF is more pronounced on the tensile strength and ductility. The tensile strength increases and the ductility decreases due to the restriction of the molecular movements caused by the CNF and also a good interaction between the matrix and the nanofibers lead to a good stress transfer from the matrix to the nanofibers.

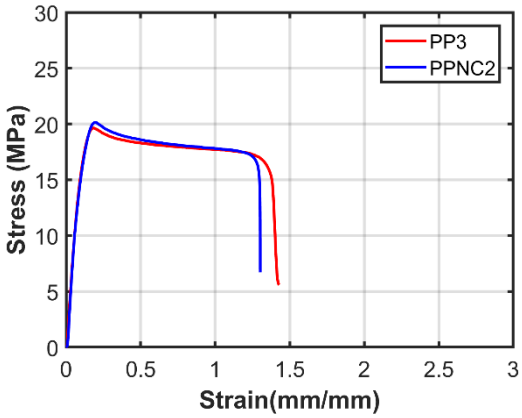

Fig. 4.4: Stress-strain curves for the comparison of the processed pure polymer (PP3) and the nanocomposite (PPNC2).

4.3.2. Thermal behavior

The thermal behavior of the processed pure polymer and its nanocomposites were studied using TGA. The values for TGA have been presented in Table 4.2 and the curves for the TGA and the derivative TGA have been shown in Fig 4.5. As can be seen from the values and the curves, the thermal stability of the polymer seem to have reduced by the addition of the nanofibers to the polymer. The difference in the values is little but shows a decreasing trend. This trend has also been seen by Paleo et al. [97] at low loading levels of the carbon nanofibers in the PP matrix. In their case, at 0.2 vol.%

loading level, the thermal stability of the polymer reduced with the addition of carbon nanofibers. But with an increase in the loading percentage, the thermal stability started to increase. This can be explained by the greater percentage of agglomeration seen in their work through SEM. Increasing the loading percentage in the future might lead to an increase in the thermal stability. The process of ultrasonic mixing could also cause shortening of the carbon nanofibers along with the scission of polymer chains. This could also have led to a reduction in the thermal stability due to lower reinforcement effect of the carbon nanofibers by shortening, which could make the polymer chain movements easier and thus lead to a reduction in the degradation temperature.

	T_{int1} (°C)	T_{onset} (°C)	T_{max} (°C)
PPNC1	353	432	466
PPNC2	354	434	471

Table 4.2: TGA values for mechanically mixed (PPNC1) and ultrasonically mixed (PPNC2) nanocomposites.

The FTIR result for the compositional analysis of the pure polymer, ultrasonically dissolved polymer and the nanocomposite have been presented in Fig 4.6. The peaks observed around 2950 cm^{-1} and 1456 cm^{-1} which verify PP, along with the other peaks, have remained consistent between all the samples. This would mean that there is no change in the chemical structure of the samples due to the processing or due to the addition of the carbon nanofibers to the matrix.

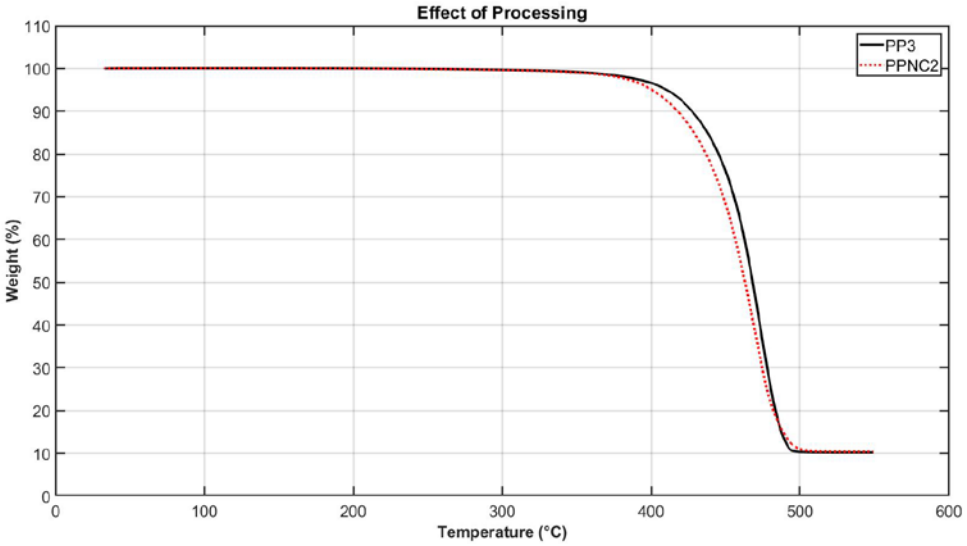

Fig. 4.5: TGA and derivative TGA curves for processed pure polymer (PP3) and the nanocomposite (PPNC2).

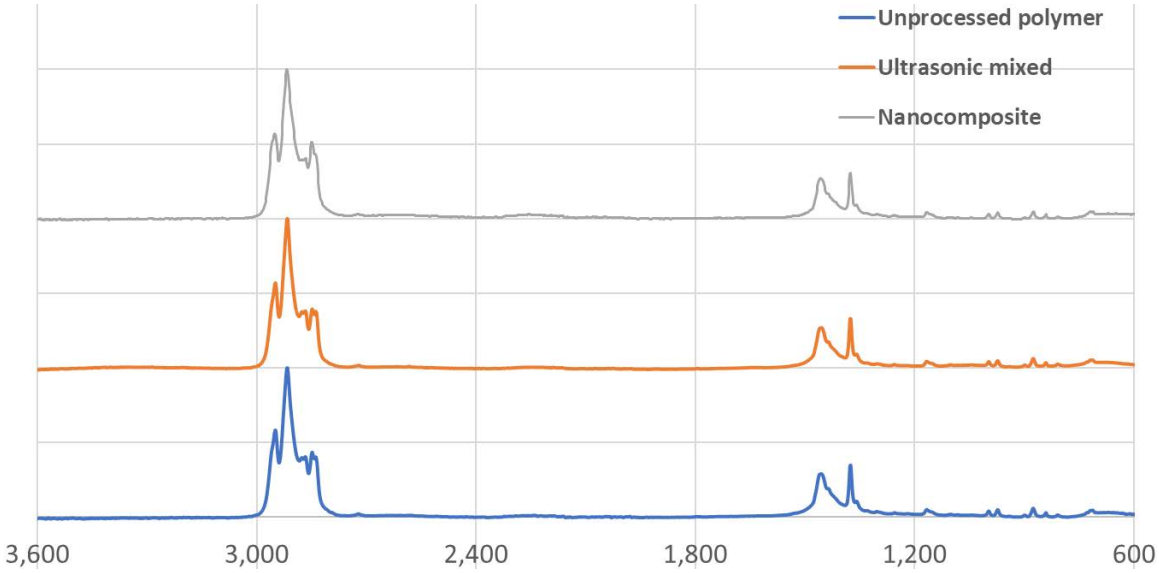

Fig. 4.6: FTIR for pure polymer (PP1), ultrasonically mixed dissolved polymer (PP3) and ultrasonically mixed nanocomposite (PPNC2)

4.4. Effect of processing and addition of nanomaterials on the strain-rate sensitivity of the polymer

The strain-rate sensitivity of PP and its nanocomposites have been studied by performing the tensile tests at varying strain rates between 10^{-4} s^{-1} and 10^{-1} s^{-1}. The results for the stress-strain properties of the polymers at varying strain rates have been shown in Fig 4.7. A strong strain-rate dependency has been shown by the polymer.

As has been explained in Chapter 2, for a semi-crystalline polymer, the α-process for stress relaxation involves two relaxation processes, one in the crystallites and the other in the amorphous zone. Stress Relaxation occurs by a chain movement through the crystallites which causes an additional shearing in the amorphous zone. As the yielding behavior of the polymer is dependent on its specific stress relaxation processes, an increase in the strain rate leads to a reduction in the ductility of the polymer. Yielding behavior of the polymer is affected by the ratio of the applied strain rates to the respective relaxation processes of the polymer, and, as this ratio increases, i.e. as the strain increases, the restriction to plastic flow increases in the polymer which leads to a brittleness in the polymer.

Stress increases or decreases as a response to the increase or decrease in the strain rate to allow for the readjustment of internal forces to maintain a linear proportional relation between the tensile stress and the strain experienced by the polymer. This means that, as the restriction to plastic flow increases with an increase in the strain rate, the stress also increases as a response to this restriction of the plastic flow. As the plastic flow experiences a restriction, the molecules become capable of handling higher loads and thus the stress increases as a result.

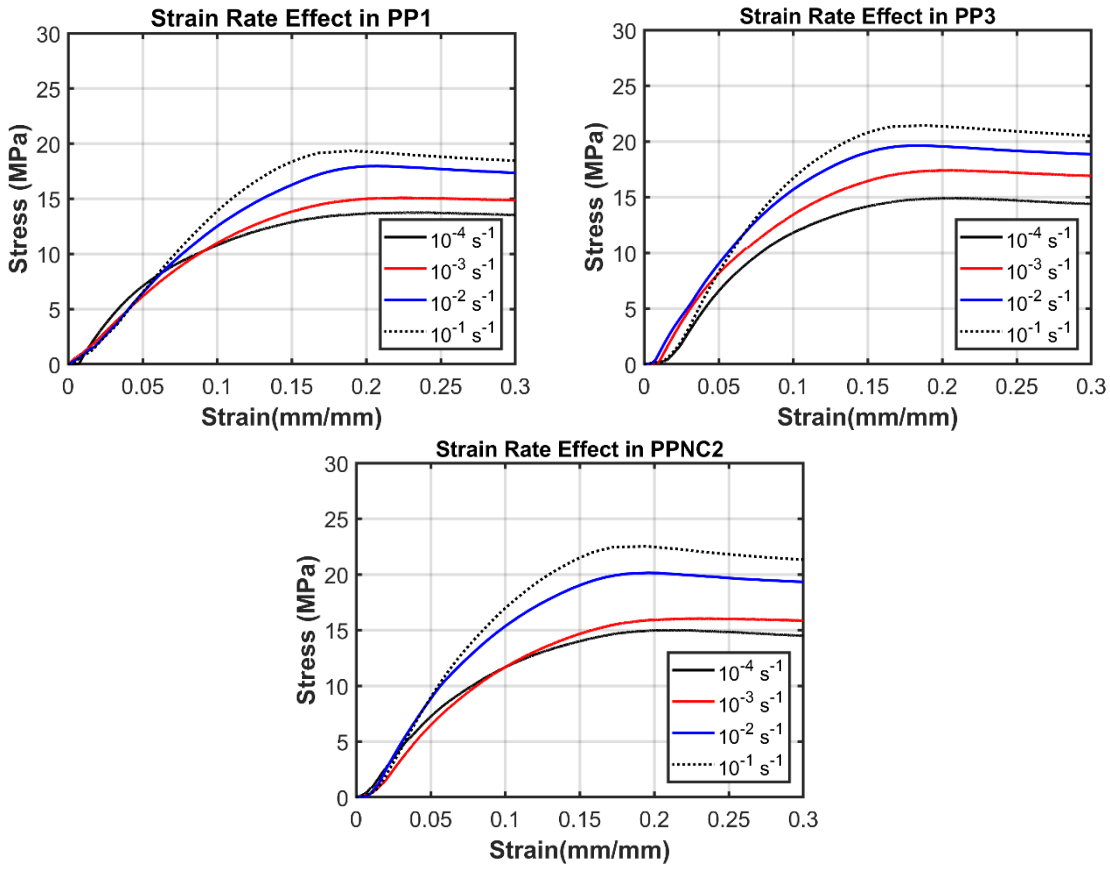

Fig 4.7: Strain rate dependency of pure polymer (PP1), processed polymer (PP3) and nanocomposites (PPNC2).

As it can be seen in Fig 4.8, the elongation at break i.e. the ductility of the polymer is reducing with an increase in the strain rate which is the same as explained above. The pure polymer, ultrasonicated polymer and its nanocomposites all follow a similar trend which is similar to the numerous studies [4,5,8,25,30,95,98] that have been done on the strain rate dependency of the polymer. Fig 4.9 shows the linear relationship between the increase in the tensile strength of the polymer with an increase in the strain rate between 10^{-4} s^{-1} and 10^{-1} s^{-1}. The linear relationship can be seen in the pure polymer, processed polymer and also in the nanocomposites.

The effect of the addition of nanofibers on the strain-rate dependency of the polymer was an interesting fact to study. As it can be seen in Fig 4.8, the nanocomposites follow the same trend as the polymers with an increase in the linearity of the strain rate dependency. On the other hand, the ductility has a non-linear decrease, with an increase in the strain rate, in all the three cases. With the addition of nanomaterials in the polymer, the non-linearity for the decrease of ductility has also been enhanced. The addition of nanomaterials serves as a reinforcement for the polymer which can further enhance the strain rate dependency of the polymer as the reinforcement would contribute to the restriction in the plastic flow of the polymer. Further studies can be done at higher strain rates to allow for the modeling of the stress-strain response of the polymer nanocomposites to understand the response of the behavior at different strain rates experienced in various applications of nanocomposites in the industry.

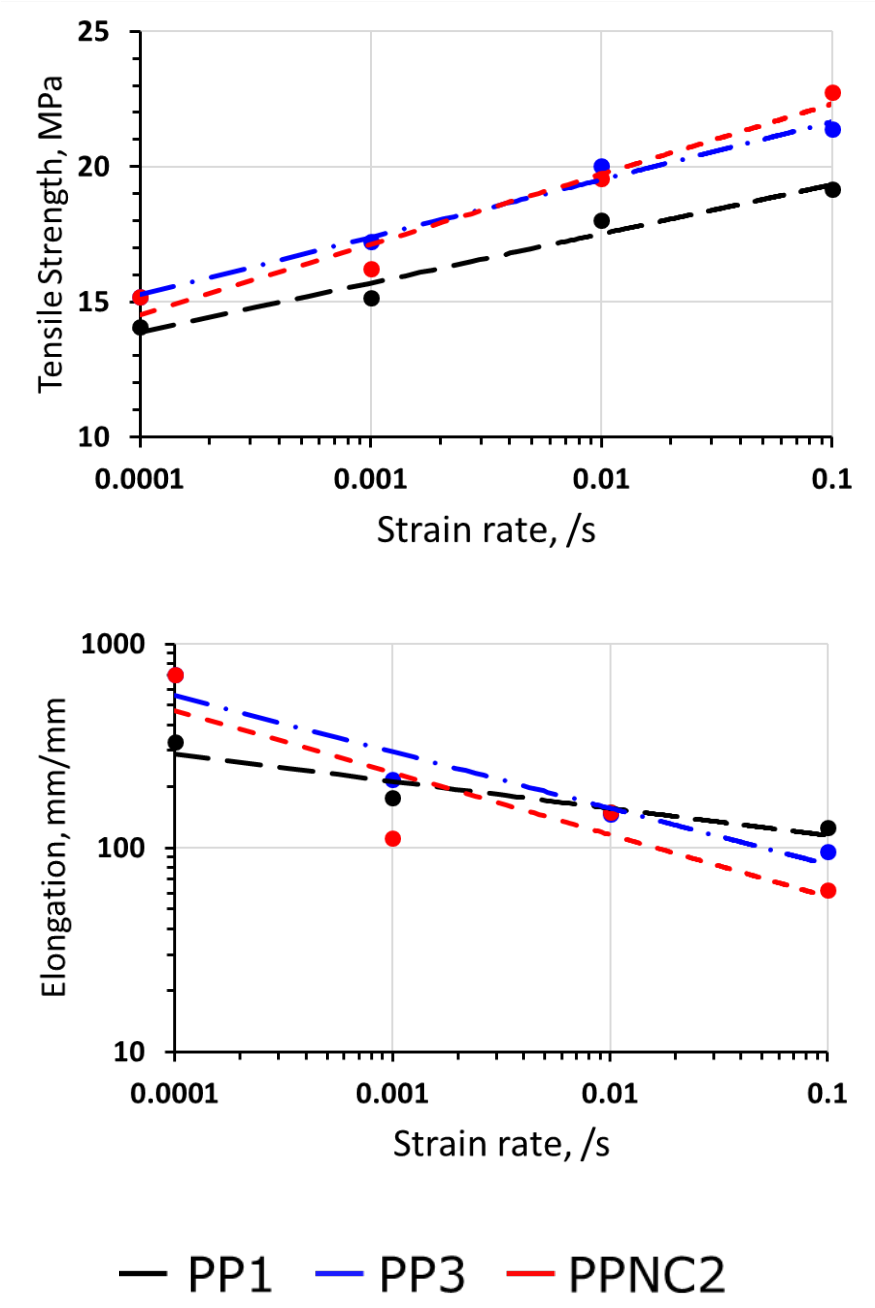

Fig. 4.8: Effect of strain-rate dependency on the tensile strength and elongation at break for pure (PP1), processed polymer (PP3) and nanocomposite (PPNC2).

CHAPTER V

CONCLUSION AND FUTURE WORKS

In this study, experimental work has been done to study the effect of ultrasonication processing, and addition of CNF on the mechanical properties and thermal behavior of PP. The effect of nanomaterial addition has been studied on the strain-rate dependency of the polymer system. The nanocomposites with carbon nanofibers have been manufactured using ultrasonic-assisted mixing and mechanical mixing, and injection molded to tensile test specimens. Mechanical properties have been studied using tensile tests and then analyzing the tensile strength and elongation at break of the polymer systems. Thermal behaviors have been studied using TGA and then analyzing the degradation temperatures of the samples.

A mold for the injection molding of the tensile test specimens has been manufactured for this work. The mold design is based on several necessary considerations and the study of the polymer flow in the mold with the help of Moldex 3D software. The shear rate values from the simulations have been used to statistically analyze the design and determine the dimensions of the injection mold using ANOVA.

PP has shown a strong strain-rate dependency with an increase in the tensile strength and the decrease in the elongation at break due to an increase in the strain rate. These responses have been studied based on the stress relaxation processes in semi-crystalline polymers and their effect on the strength and ductility of these polymers. The fabricated nanocomposites also show a similar trend of strain-rate dependency with a similar linearity in the increase of tensile strength with an increase in the strain rate. The

tensile strength and elongation of the polymer has not been affected much by the addition of nanofibers, while the thermal stability has reduced due to the low loading levels of the nanofibers in this study.

The effects of ultrasonic-assisted mixing on PP have been analyzed for polymer degradation caused by cavitation in a solution. There is a visible effect of the degradation of the polymer due to ultrasonication, as seen in the mechanical properties and thermal behaviors of the processed polymer. But ultrasonication has not caused an overall detrimental effect on the mechanical properties of the sample, as compared to other works in the literature, due to other reasons such as the interaction of the mineral filler in the polymer. The overall observations from this work can be summarized as follows:

- Tensile strength of the polymer and its nanocomposites increase linearly with an increase in the quasi-static strain rate, with a simultaneous decrease in the ductility.
- The effect of polymer degradation caused by ultrasonication in the manufacture of nanocomposites depends on factors such as presence/absence of fillers, variations of processing time, and the molecular weight of the polymer.
- Along with the mechanical properties of the nanomaterials, a percentage of carbon nanofibers in the polymer matrix is a crucial factor in determining their reinforcement effect on the polymer when ultrasonication is used for their manufacture.

CHAPTER VI

FUTURE WORKS

Based on the observations and results of this study, some future work is necessary to determine the exact cause of the effects seen in the polymer due to the processing and the addition of the nanomaterials in the polymer matrix. These future works have been mentioned below:

1. To further understand and model the strain-rate dependency of the polymer and the nanocomposites, higher strain-rate levels up to the order of 10^4 s^{-1} must be studied using servo-hydraulic machines and Split Hopkinson Pressure Bar tests.
2. For understanding the effect of addition of nanomaterials using ultrasonication on the mechanical properties and thermal behavior, different loading levels of the CNF must be utilized. TGA can then be used to see the effect of variation in the loading level on the thermal stability of the polymer.
3. To study the effect of orientation of the nanofibers in the polymer matrix, the processed nanocomposites can be extruded/drawn as this would align the fibers. The changes in alignment can be analyzed with the help of scanning electron microscopy (SEM) and transmission electron microscopy (TEM).
4. The effect of processing time in ultrasonic processing of nanocomposites can be studied by doing a time variation study. SEM and TEM can be used to study the changes in the dispersion and Differential Scanning Calorimetry (DSC) can also be employed to see a change in the crystallinity of the polymer due to the processing.

References

[1] Luo, J. J. J., and Daniel, I. M. I., 2003, "Characterization and Modeling of Mechanical Behavior of Polymer/clay Nanocomposites," Compos. Sci. Technol., **63**(11), pp. 1607–1616.

[2] Thostenson, E. T., Li, C., and Chou, T., 2005, "Nanocomposites in Context," Compos. Sci. Technol., **65**(March 2005), pp. 491–516.

[3] Hussain, F., 2006, "Polymer-Matrix Nanocomposites, Processing, Manufacturing, and Application: An Overview," J. Compos. Mater., **40**(17), pp. 1511–1575.

[4] Zrida, M., Laurent, H., Grolleau, V., Rio, G., Khlif, M., Guines, D., Masmoudi, N., and Bradai, C., 2010, "High-Speed Tensile Tests on a Polypropylene Material," Polym. Test., **29**(6), pp. 685–692.

[5] Schobig, M., Bierogel, C., Grellmann, W., and Mecklenburg, T., 2008, "Mechanical Behavior of Glass-Fiber Reinforced Thermoplastic Materials under High Strain Rates," Polym. Test., **27**(7), pp. 893–900.

[6] Duan, S., Mo, F., Yang, X., Tao, Y., Wu, D., and Peng, Y., 2016, "Experimental and Numerical Investigations of Strain Rate Effects on Mechanical Properties of LGFRP Composite," Compos. Part B Eng., **88**, pp. 101–107.

[7] Hufenbach, W., Langkamp, A., Gude, M., Ebert, C., Hornig, A., Nitschke, S., and Böhm, H., 2013, "Characterisation of Strain Rate Dependent Material Properties of Textile Reinforced Thermoplastics for Crash and Impact Analysis," Procedia Mater. Sci., **2**, pp. 204–211.

[8] Şerban, D. A., Weber, G., Marşavina, L., Silberschmidt, V. V., and Hufenbach, W., 2013, "Tensile Properties of Semi-Crystalline Thermoplastic Polymers: Effects of Temperature and Strain Rates," Polym. Test., **32**(2), pp. 413–425.

[9] Bardenheier, R., and Rogers, G., 2006, "Dynamic Impact Testing with Servohydraulic Testing Machines," J. Phys. IV, **134**, pp. 693–699.

[10] Martini, S., 2013, "Sonocrystallization of Fats," *Sonocrystallization of Fats*, Springer New York, New York, NY, pp. 41–62.

[11] Leighton, T. ., 1995, "Bubble Population Phenomena in Acoustic Cavitation," Ultrason. Sonochem., **2**(2), pp. S123–S136.

[12] Eskin, G., and Eskin, D., 2014, *Ultrasonic Treatment of Light Alloy Melts*.

[13] Merouani, S., Hamdaoui, O., and Rezgui, Y., 2015, "Optimum Bubble Temperature for the Production of Hydroxyl Radical in Acoustic Cavitation–Frequency Dependence," Acta Acust. united.

[14] Doulah, M. S., 1978, "A Proposed Mechanism for the Degradation of Addition

Polymers in Cavitating Ultrasonic Fields," J. Appl. Polym. Sci., **22**(6), pp. 1735–1743.

[15] Buchholz, B. A., Zahn, J. M., Kenward, M., Slater, G. W., and Barron, A. E., 2004, "Flow-Induced Chain Scission as a Physical Route to Narrowly Distributed, High Molar Mass Polymers," Polymer (Guildf)., **45**(4), pp. 1223–1234.

[16] Suslick, K. S., and Price, G. J., 1999, "APPLICATIONS OF ULTRASOUND TO MATERIALS CHEMISTRY," Annu. Rev. Mater. Sci, **29**, pp. 295–326.

[17] Flosdorf, E. W., and Chambers, L. A., 1933, "THE CHEMICAL ACTION OF AUDIBLE SOUND," J. Am. Chem. Soc., **55**(7), pp. 3051–3052.

[18] Price, G. J., Hearn, M. P., Wallace, E. N. K., and Patel, A. M., 1996, "Ultrasonically Assisted Synthesis and Degradation of Poly(dimethyl Siloxane)," Polymer (Guildf)., **37**(12), pp. 2303–2308.

[19] Koda, S., Mori, H., Matsumoto, K., and Nomura, H., 1994, "Ultrasonic Degradation of Water-Soluble Polymers," Polymer (Guildf)., **35**(1), pp. 30–33.

[20] O'shea, J., and Bradbury, J., 1973, "The Effect of Ultrasonic Irradiation on Proteins," Aust. J. Biol. Sci., **26**(3), p. 583.

[21] Freifelder, D., and Davison, P. F., 1962, "Studies on the Sonic Degradation of Deoxyribonucleic Acid," Biophys. J., **2**(3), pp. 235–247.

[22] Bower, D. I., 2002, *An Introduction to Polymer Physics*, Cambridge University Press, Cambridge.

[23] Strobl, G., 2007, *The Physics of Polymers: Concepts for Understanding Their Structures and Behavior*, Springer Berlin Heidelberg, Berlin, Heidelberg.

[24] Ree, T., and Eyring, H., 1955, "Theory of Non-Newtonian Flow. I. Solid Plastic System," J. Appl. Phys., **26**(7), pp. 793–800.

[25] Mulliken, A. D., and Boyce, M. C., 2006, "Mechanics of the Rate-Dependent Elastic-Plastic Deformation of Glassy Polymers from Low to High Strain Rates," Int. J. Solids Struct., **43**(5), pp. 1331–1356.

[26] Boyce, M. C., Parks, D. M., and Argon, A. S., 1988, "Large Inelastic Deformation of Glassy Polymers. Part I: Rate Dependent Constitutive Model," Mech. Mater., **7**(1), pp. 15–33.

[27] Pouriayevali, H., Arabnejad, S., Guo, Y. B., and Shim, V. P. W., 2013, "A Constitutive Description of the Rate-Sensitive Response of Semi-Crystalline Polymers," Int. J. Impact Eng., **62**, pp. 35–47.

[28] Bles, G., Nowacki, W. K., and Tourabi, A., 2009, "Experimental Study of the Cyclic Visco-Elasto-Plastic Behaviour of a Polyamide Fibre Strap," Int. J. Solids Struct., **46**(13), pp. 2693–2705.

[29] Vandenbroucke, A., Laurent, H., Aït Hocine, N., and Rio, G., 2010, "A Hyperelasto-Visco-Hysteresis Model for an Elastomeric Behaviour: Experimental and Numerical Investigations," Comput. Mater. Sci., **48**(3), pp. 495–503.

[30] Gensler, R., Plummer, C. J. G., Grein, C., and Kausch, H. H., 2000, "Influence of the Loading Rate on the Fracture Resistance of Isotactic Polypropylene and Impact Modified Isotactic Polypropylene," Polymer (Guildf)., **41**(10), pp. 3809–3819.

[31] Duan, Y., Saigal, A., Greif, R., and Zimmerman, M., 2001, "A Uniform Phenomenological Constitutive Model for Glassy and Semicrystalline Polymers," Polym. Eng. Sci., **41**(8).

[32] G'sell, C., and Jonas, J. J., 1979, "Determination of the Plastic Behaviour of Solid Polymers at Constant True Strain Rate," J. Mater. Sci., **14**(3), pp. 583–591.

[33] G'sell, C., Aly-Helal, N. A., and Jonas, J. J., 1983, "Effect of Stress Triaxiality on Neck Propagation during the Tensile Stretching of Solid Polymers," J. Mater. Sci., **18**(6), pp. 1731–1742.

[34] Schang, O., Billon, N., Muracciole, J. M., and Fernagut, F., 1996, "Mechanical Behavior of a Ductile Polyamide 12 during Impact," Polym. Eng. Sci., **36**(4), pp. 541–550.

[35] Mason, T. J., and Peters, D., *Practical Sonochemistry : Uses and Applications of Ultrasound*.

[36] Tayal, A., and Khan, S. A., 2000, "Degradation of a Water-Soluble Polymer: Molecular Weight Changes and Chain Scission Characteristics," Macromolecules, **33**(26), pp. 9488–9493.

[37] Bhanvase, B. A., and Sonawane, S. H., 2014, "Ultrasound Assisted in Situ Emulsion Polymerization for Polymer Nanocomposite: A Review," Chem. Eng. Process. Process Intensif., **85**, pp. 86–107.

[38] Gedanken, A., 2004, "Using Sonochemistry for the Fabrication of Nanomaterials," **11**, pp. 47–55.

[39] Yasmin, A., Luo, J. J., and Daniel, I. M., 2006, "Processing of Expanded Graphite Reinforced Polymer Nanocomposites," Compos. Sci. Technol., **66**(9), pp. 1179–1186.

[40] Safadi, B., Andrews, R., and Grulke, E. A., 2002, "Multiwalled Carbon Nanotube Polymer Composites: Synthesis and Characterization of Thin Films," J. Appl. Polym. Sci., **84**(14), pp. 2660–2669.

[41] Zhang, K., Park, B. J., Fang, F. F., and Choi, H. J., 2009, "Sonochemical Preparation of Polymer Nanocomposites," Molecules, **14**(6), pp. 2095–2110.

[42] Gupta, R. K., Kennel, E., and Kim, K.-L., 2010, "Polymer Nanocomposites

Handbook," p. 566.

[43] Leaversuch, R., 2001, "Nanocomposites Broaden Roles in Automotive, Barrier Packaging," Platics Technol. Online, pp. 64–69.

[44] NIST, 2005, "BFRL," NIST [Online]. Available: http://www.bfrl.nist.gov/Annual/2004-2005/BFRL06.pdf.

[45] Baeza, F., Galao, O., Zornoza, E., and Garcés, P., 2013, "Multifunctional Cement Composites Strain and Damage Sensors Applied on Reinforced Concrete (RC) Structural Elements," Materials (Basel)., **6**(3), pp. 841–855.

[46] Du, J.-H., Sun, C., Bai, S., Su, G., Ying, Z., and Cheng, H.-M., 2002, "Microwave Electromagnetic Characteristics of a Microcoiled Carbon Fibers/paraffin Wax Composite in Ku Band," J. Mater. Res., **17**(5), pp. 1232–1236.

[47] Endo, M., Kim, Y. A., Hayashi, T., Nishimura, K., Matusita, T., and Miyashita, K. ., 2001, "Vapor-Grown Carbon Fibers (VGCFs): Basic Properties and Their Battery Applications," Carbon N. Y., **39**(9), pp. 1287–1297.

[48] Al-Saleh, M. H., and Sundararaj, U., 2009, "A Review of Vapor Grown Carbon Nanofiber/polymer Conductive Composites," Carbon N. Y., **47**(1), pp. 2–22.

[49] Tibbetts, G. G., Devour, M. G., and Rodda, E. J., 1987, "An Adsorption-Diffusion Isotherm and Its Application to the Growth of Carbon Filaments on Iron Catalyst Particles," Carbon N. Y., **25**(3), pp. 367–375.

[50] Endo, M., Shikata, M., Momose, T., and Shiraishi, M., 1985, "Vapor Grown Carbon Fibers Obtained by Fluid Ultra Fine Catalytic Particles," *17th Biennial Carbon Conference Proceedings, Lexington, Ky, USA: American Carbon Society.*, pp. 295–296.

[51] Tibbetts, G. G., Bernardo, C. A., Gorkiewicz, D. W., and Alig, R. L., 1994, "Role of Sulfur in the Production of Carbon Fibers in the Vapor Phase," Carbon N. Y., **32**(4), pp. 569–576.

[52] Tibbetts, G. G., Gorkiewicz, D. W., and Alig, R. L., 1993, "A New Reactor for Growing Carbon Fibers from Liquid- and Vapor-Phase Hydrocarbons," Carbon N. Y., **31**(5), pp. 809–814.

[53] Inagaki, M., Yang, Y., and Kang, F., 2012, "Carbon Nanofibers Prepared via Electrospinning," Adv. Mater., **24**(19), pp. 2547–2566.

[54] Zhang, L., Aboagye, A., Kelkar, A., Lai, C., and Fong, H., 2014, "A Review: Carbon Nanofibers from Electrospun Polyacrylonitrile and Their Applications," J. Mater. Sci., **49**(2), pp. 463–480.

[55] Ge, M., and Sattler, K., 1994, "Observation of Fullerene Cones," Chem. Phys. Lett., **220**(3–5), pp. 192–196.

[56] Al-Saleh, M. H., and Sundararaj, U., 2011, “Review of the Mechanical Properties of Carbon Nanofiber/polymer Composites,” Compos. Part A Appl. Sci. Manuf., **42**(12), pp. 2126–2142.

[57] Teo, K. B. K., Singh, C., Chhowalla, M., and Milne, W. I., 2003, “Catalytic Synthesis of Carbon Nanotubes and Nanofibers,” Encycl. Nanosci. Nanotechnol., **X**, pp. 1–22.

[58] Palmeri, M. J., Putz, K. W., Ramanathan, T., and Brinson, L. C., 2011, “Multi-Scale Reinforcement of CFRPs Using Carbon Nanofibers,” Compos. Sci. Technol., **71**(2), pp. 79–86.

[59] Kim, Y. A., Hayashi, T., Endo, M., and Dresselhaus, M. S., 2013, “Carbon Nanofibers,” *Springer Handbook of Nanomaterials*, Springer Berlin Heidelberg, Berlin, Heidelberg, pp. 233–262.

[60] Coquay, P., Flahaut, E., De Grave, E., Peigney, A., Vandenberghe, R. E., and Laurent, C., 2005, “Fe/Co Alloys for the Catalytic Chemical Vapor Deposition Synthesis of Single- And Double-Walled Carbon Nanotubes (CNTs). 2. the CNT-Fe/Co-MgAl 2O4 System,” J. Phys. Chem. B, **109**(38), pp. 17825–17830.

[61] Lee, B. O., Woo, W. J., and Kim, M.-S., 2001, “EMI Shielding Effectiveness of Carbon Nanofiber Filled Poly(vinyl Alcohol) Coating Materials,” Macromol. Mater. Eng., **286**(2), pp. 114–118.

[62] Kuriger, R. J., and Alam, M. K., 2001, “Extrusion Conditions and Properties of Vapor Grown Carbon Fiber Reinforced Polypropylene,” Polym. Compos., **22**(5), pp. 604–612.

[63] Tibbetts, G. G., Lake, M. L., Strong, K. L., and Rice, B. P., 2007, “A Review of the Fabrication and Properties of Vapor-Grown Carbon Nanofiber/polymer Composites,” Compos. Sci. Technol., **67**(7–8), pp. 1709–1718.

[64] Glasgow, D. G., Tibbetts, G. G., Matuszewski, J. J., and Walters, K. R., 2004, “Surface Treatment of Carbon Nanofibers for Improved Composite Mechanical Properties.,” *International Society for Advancement of Materials and Process Engineering (SAMPE) Symposium and Exhibition, Long Beach, CA*, pp. 16–20.

[65] Lafdi, K., and Matzek, M., 2003, “Carbon Nanofibers as a Nano-Reinforcement for Polymeric Nanocomposites.,” *48th International SAMPE Symposium Proceedings, Long Beach, USA*.

[66] Breuer, O., and Sundararaj, U., 2004, “Big Returns from Small Fibers: A Review of Polymer/carbon Nanotube Composites,” Polym. Compos.

[67] Finegan, I. C., and Tibbetts, G. G., 2001, “Electrical Conductivity of Vapor-Grown Carbon Fiber/thermoplastic Composites,” J. Mater. Res., **16**(6), pp. 1668–1674.

[68] Tibbetts, G. G., and Beetz, C. P., 1987, “Mechanical Properties of Vapour-Grown

Carbon Fibres," J. Phys. D Appl. Phys. J. Phys. D Appl. Phys, **20**(20), pp. 292–292.

[69] Patton, R. D., Pittman, C. U., Wang, L., and Hill, J. R., 1999, "Vapor Grown Carbon Fiber Composites with Epoxy and Poly(phenylene Sulfide) Matrices," Compos. Part A Appl. Sci. Manuf., **30**(9), pp. 1081–1091.

[70] Lozano, K., 2000, "Vapor-Grown Carbon-Fiber Composites: Processing and Electrostatic Dissipative Applications," Jom, **52**(11), pp. 34–36.

[71] Kim, P., Shi, L., Majumdar, A., and McEuen, P. L., 2001, "Thermal Transport Measurements of Individual Multiwalled Nanotubes," pp. 2–5.

[72] Berber, S., Kwon, Y.-K., and Tomanek, D., 2000, "Unusually High Thermal Conductivity of Carbon Nanotubes," pp. 1–4.

[73] Subramanian, V., Zhu, H., and Wei, B., 2006, "High Rate Reversibility Anode Materials of Lithium Batteries from Vapor-Grown Carbon Nanofibers," pp. 7178–7183.

[74] Kilbride, B. E., Coleman, J. N., Fraysse, J., Fournet, P., Cadek, M., Drury, A., Hutzler, S., Roth, S., and Blau, W. J., 2002, "Experimental Observation of Scaling Laws for Alternating Current and Direct Current Conductivity in Polymer-Carbon Nanotube Composite Thin Films," J. Appl. Phys., **92**(7), pp. 4024–4030.

[75] Biercuk, M. J., Llaguno, M. C., Radosavljevic, M., Hyun, J. K., Johnson, A. T., and Fischer, J. E., 2002, "Carbon Nanotube Composites for Thermal Management," Appl. Phys. Lett., **80**(15), pp. 2767–2769.

[76] W.D.Callister, J., 2003, *Materials Science and Engineering: An Introduction*, Wiley, New York.

[77] Baddour, C. E., and Briens, C., 2005, "I NTERNATIONAL J OURNAL OF C HEMICAL Carbon Nanotube Synthesis : A Review Carbon Nanotube Synthesis : A Review," **3**.

[78] Bikiaris, D., 2010, "Microstructure and Properties of Polypropylene/carbon Nanotube Nanocomposites," Materials (Basel)., **3**(4), pp. 2884–2946.

[79] Hata, K., Futaba, D. N., Mizuno, K., and Namai, T., 2012, "Water-Assisted Highly Efficient Synthesis of Impurity-Free Single-Walled Carbon Nanotubes," **1362**(2004).

[80] Wong, E. W., Sheehan, P. E., and Lieber, C. M., 1997, "Nanobeam Mechanics: Elasticity, Strength, and Toughness of Nanorods and Nanotubes," Science (80-.)., **277**(5334), pp. 1971–1975.

[81] Yu, M., 2000, "Strength and Breaking Mechanism of Multiwalled Carbon Nanotubes Under Tensile Load," Science (80-.)., **287**(5453), pp. 637–640.

[82] Ramanathan, T., Liu, H., and Brinson, L. C., 2005, "Functionalized SWNT/polymer Nanocomposites for Dramatic Property Improvement," J. Polym. Sci. Part B Polym. Phys., **43**(17), pp. 2269–2279.

[83] Meo, M., and Rossi, M., 2006, "Prediction of Young's Modulus of Single Wall Carbon Nanotubes by Molecular-Mechanics Based Finite Element Modelling," Compos. Sci. Technol., **66**(11–12), pp. 1597–1605.

[84] ASTM D638, 2004, "Standard Test Method for Tensile Properties of Plastics," Annu. B. ASTM Stand., pp. 1–15.

[85] Pasumarthi, P., Absar, S., and Choi, H., 2016, "The Effect of Geometrical Parameters on the Characteristics of Ultrasonic Processing for Metal Matrix Nanocomposites (MMNCs)," J. Manuf. Process., **24**, pp. 382–390.

[86] Chen, X., Wei, S., Yadav, A., Patil, R., Zhu, J., Ximenes, R., Sun, L., and Guo, Z., 2011, "Poly (Propylene)/ Carbon Nanofiber Nanocomposites : Ex Situ Solvent-Assisted Preparation and Analysis of Electrical and Electronic Properties," pp. 434–443.

[87] Li, Y., Zhu, J., Wei, S., Ryu, J., Wang, Q., and Sun, L., "Poly (Propylene) Nanocomposites Containing Various Carbon Nanostructures," pp. 2429–2438.

[88] Turi, E. A., 1981, *Thermal Characterization of Polymeric Materials*, Academic Press.

[89] Kim, J. Y., Kim, D. K., and Kim, S. H., 2009, "Thermal Decomposition Behavior of Poly(ethylene 2,6-Naphthalate)/silica Nanocomposites," Polym. Compos., **30**(12), pp. 1779–1787.

[90] Li, X.-G., and Huang, M.-R., 1999, "Thermal Degradation of Kevlar Fiber by High-Resolution Thermogravimetry," J. Appl. Polym. Sci., **71**(4), pp. 565–571.

[91] Li, X. H., Tjong, S. C., Meng, Y. Z., and Zhu, Q., 2003, "Fabrication and Properties of Poly (Propylene Carbonate)/Calxium Carbonate Composites," J. Polym. Sci. Part B Polym. Phys., **41**(15), pp. 1806–1813.

[92] Adur, A. M., Constable, R. C., and Humenik, J. A., 1988, "Use of Acrylic Acid-Modified Polyolefins to Improve Performance Properties of Mica Filled Polyolefins," J. Thermoplast. Compos. Mater., **1**(April 1998), pp. 196–205.

[93] Tabtiang, A., and Venables, R., 2017, "Reactive Surface Treatment for Calcium Carbonate Filler in Polypropylene," **6440**(November).

[94] Hasan, M. M., Zhou, Y., and Jeelani, S., 2007, "Thermal and Tensile Properties of Aligned Carbon Nanofiber Reinforced Polypropylene," Mater. Lett., **61**(4–5), pp. 1134–1136.

[95] Ingram, J., Zhou, Y., Jeelani, S., Lacy, T., and Horstemeyer, M. F., 2008, "Effect

of Strain Rate on Tensile Behavior of Polypropylene and Carbon Nanofiber Filled Polypropylene," Mater. Sci. Eng. A, **489**(1–2), pp. 99–106.

[96] Sui, G., Zhong, W.-H., Fuqua, M. a., and Ulven, C. a., 2007, "Crystalline Structure and Properties of Carbon Nanofiber Composites Prepared by Melt Extrusion," Macromol. Chem. Phys., **208**(17), pp. 1928–1936.

[97] Paleo, A. J., Sencadas, V., van Hattum, F. W. J., Lanceros-Méndez, S., and Ares, A., 2013, "Carbon Nanofiber Type and Content Dependence of the Physical Properties of Carbon Nanofiber Reinforced Polypropylene Composites," Polym. Eng. Sci.

[98] Dasari, A., and Misra, R. D. K., 2003, "On the Strain Rate Sensitivity of High Density Polyethylene and Polypropylenes," Mater. Sci. Eng. A, **358**(1–2), pp. 356–371.

APPENDICES

Appendix A

Design of Injection Mold

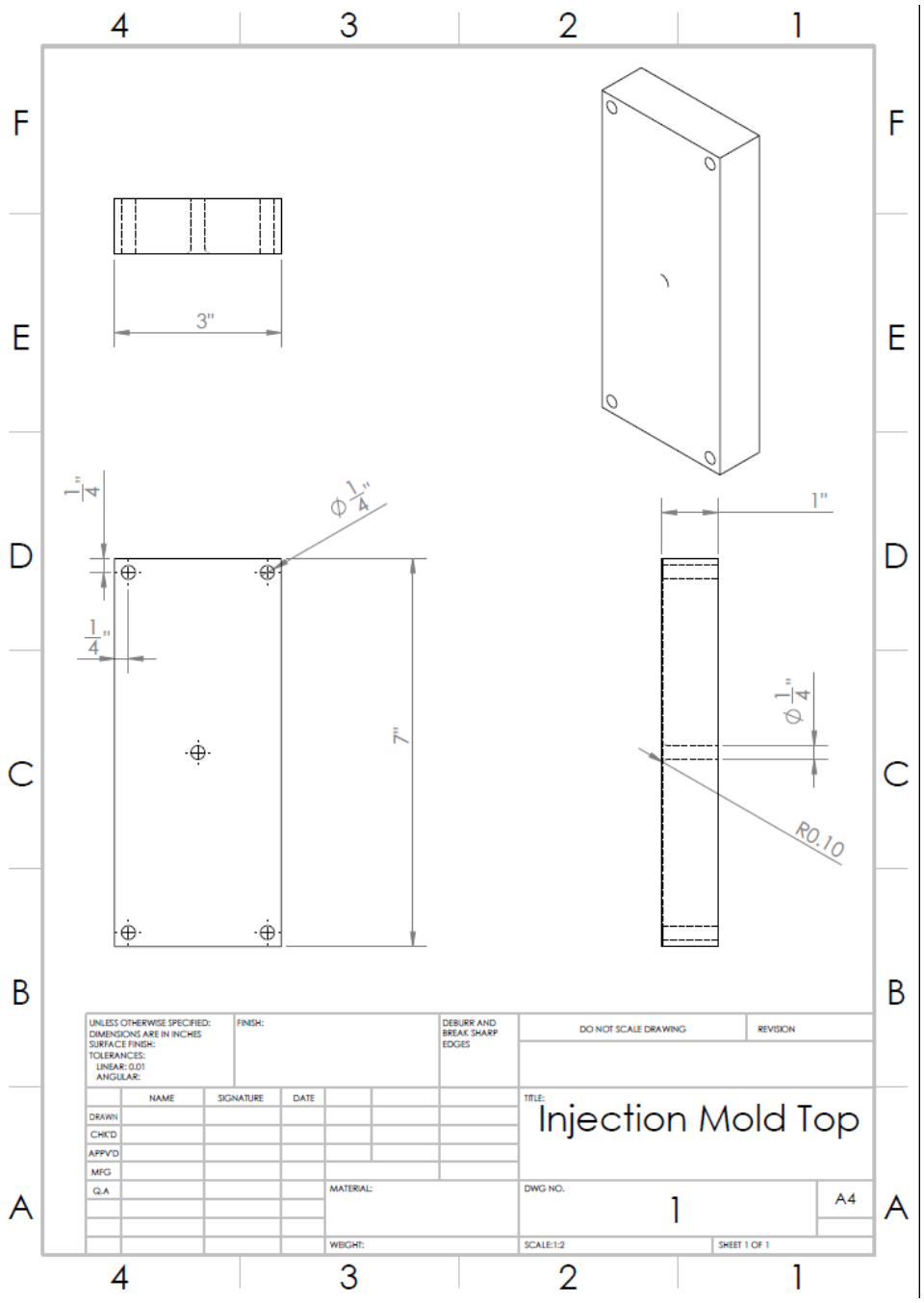

Fig. A.1: Design of Injection mold – Part A

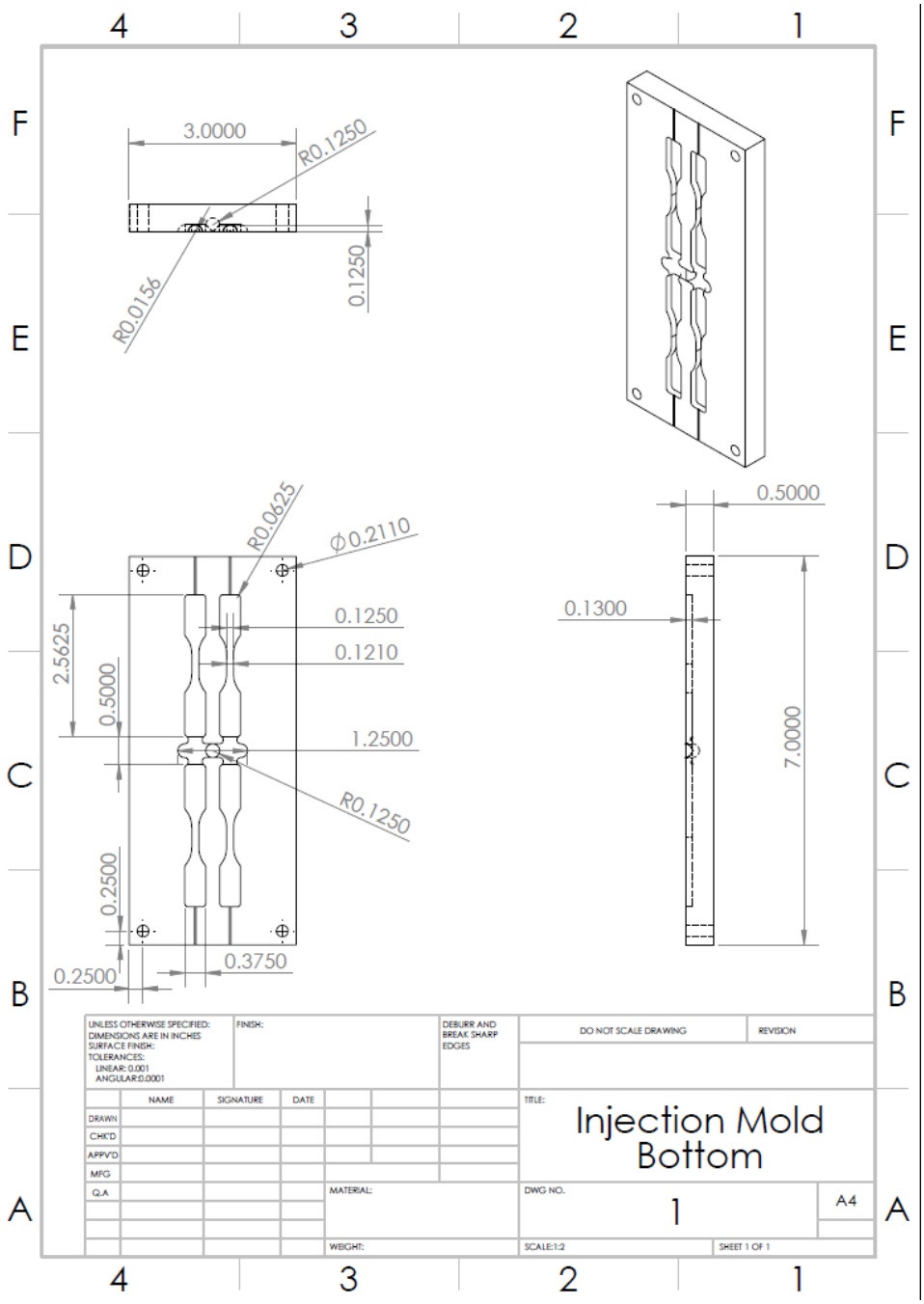

Fig. A.2: Design of Injection mold – Part B

Appendix A

ANOVA results for Shear Rate analysis

Effects Pareto for Shear Rate

Results for: Worksheet 1

Factorial Regression: Shear Rate versus Runner Diameter, Runner Length

Analysis of Variance

Source	DF	Adj SS	Adj MS	F-Value	P-Value
Model	3	7525.26	2508.42	*	*
Linear	2	7513.25	3756.63	*	*
Runner Diameter	1	231.19	231.19	*	*
Runner Length	1	7282.06	7282.06	*	*
2-Way Interactions	1	12.01	12.01	*	*
Runner Diameter*Runner Length	1	12.01	12.01	*	*
Error	0	*	*		
Total	3	7525.26			

Model Summary

S	R-sq	R-sq(adj)	R-sq(pred)
*	100.00%	*	*

Coded Coefficients

Term	Effect	Coef	SE Coef	T-Value	P-Value	VIF
Constant		1227	*	*	*	
Runner Diameter	15.205	7.602	*	*	*	1.00
Runner Length	85.34	42.67	*	*	*	1.00
Runner Diameter*Runner Length	-3.465	-1.732	*	*	*	1.00

Regression Equation in Uncoded Units

Shear Rate = 1227 + 7.602 Runner Diameter + 42.67 Runner Length
- 1.732 Runner Diameter*Runner Length

Alias Structure

Factor	Name
A	Runner Diameter
B	Runner Length

Aliases

I
A
B
AB

Effects Pareto for Shear Rate

Factorial Regression: Shear Rate versus Runner Diameter, Runner Length

Analysis of Variance

Source	DF	Adj SS	Adj MS	F-Value	P-Value
Model	2	7513.25	3756.63	312.89	0.040
Linear	2	7513.25	3756.63	312.89	0.040
Runner Diameter	1	231.19	231.19	19.26	0.143
Runner Length	1	7282.06	7282.06	606.52	0.026
Error	1	12.01	12.01		
Total	3	7525.26			

Model Summary

S	R-sq	R-sq(adj)	R-sq(pred)
3.465	99.84%	99.52%	97.45%

Coded Coefficients

Term	Effect	Coef	SE Coef	T-Value	P-Value	VIF
Constant		1227.13	1.73	708.30	0.001	
Runner Diameter	15.20	7.60	1.73	4.39	0.143	1.00
Runner Length	85.34	42.67	1.73	24.63	0.026	1.00

Regression Equation in Uncoded Units

Shear Rate = 1227.13 + 7.60 Runner Diameter + 42.67 Runner Length

Alias Structure

Factor	Name
A	Runner Diameter
B	Runner Length

Aliases

I
A
B

Effects Pareto for Shear Rate

Factorial Regression: Shear Rate versus Runner Diameter, Runner Length

Analysis of Variance

Source	DF	Adj SS	Adj MS	F-Value	P-Value
Model	2	7513.25	3756.63	312.89	0.040
Linear	2	7513.25	3756.63	312.89	0.040
Runner Diameter	1	231.19	231.19	19.26	0.143
Runner Length	1	7282.06	7282.06	606.52	0.026
Error	1	12.01	12.01		
Total	3	7525.26			

Model Summary

S	R-sq	R-sq(adj)	R-sq(pred)
3.465	99.84%	99.52%	97.45%

Coded Coefficients

Term	Effect	Coef	SE Coef	T-Value	P-Value	VIF
Constant		1227.13	1.73	708.30	0.001	
Runner Diameter	15.20	7.60	1.73	4.39	0.143	1.00
Runner Length	85.34	42.67	1.73	24.63	0.026	1.00

Regression Equation in Uncoded Units

Shear Rate = 1227.13 + 7.60 Runner Diameter + 42.67 Runner Length

Alias Structure

Factor	Name
A	Runner Diameter
B	Runner Length